Chauveau, D., Boyden, P., Desfromont, F., Scardino, G., Scicchitano, G., Mijts, E., et al. (2026). Unraveling the spatial variability of fossil coral reef morphology on Aruba and the implications for paleo sea level estimates. *Journal of Geophysical Research: Earth Surface*, 131, e2025JF008384. https://doi.org/10.1029/2025JF008384

Unravelling the spatial variability of fossil coral reef morphology on Aruba and the implications for paleo sea level estimates

Denovan Chauveau*[a,b], Patrick Boyden[c], Florent Desfromont[d], Giovanni Scardino[e,f], Giovanni Scicchitano[e,f], Eric Mijts[g], Sonia Bejarano[h], Silas Dean[b], Ciro Cerrone[b], Alessio Rovere[b,c]

[a]Geo-Ocean, Univ Brest, CNRS, Ifremer, UMR6538, F-29280 Plouzané, France
[b]Department of Environmental Sciences, Informatics and Statistics, Ca Foscari University of Venice, Italy
[c]MARUM, Center for Marine Environmental Sciences, University of Bremen, Germany
[d]Beicip-Franlab, Rueil-Malmaison, France
[e]Department of Earth and Geo-environmental Sciences, University of Bari Aldo Moro, 70125 Bari, Italy
[f]Interdepartmental Research Center for Coastal Dynamics, University of Bari Aldo Moro, 70125 Bari, Italy
[g]University of Aruba, Oranjestad, Aruba
[h]Reef Systems Research Group, Leibniz Centre for Tropical Marine Research (ZMT), Bremen, Germany

*Corresponding author: Denovan.Chauveau@ifremer.fr
Contributing authors: pboyden@marum.de; florent.verdiere@gmail.com; giovanni.scardino@uniba.it; giovanni.scicchitano@uniba.it; eric.mijts@ua.aw; sonia.bejarano@leibniz-zmt.de; silas.dean@unive.it; ciro.cerrone@unive.it; alessio.rovere@unive.it

Keywords

Stratigraphic forward modelling; Fossil coral reef; Sea level; Marine Isotope Stage 5e; Caribbean Last Interglacial reefs

Abstract

The morphology of a coral reef terrace is a key parameter in the interpretation and quantification of past sea-level changes, but it is directly influenced by local morphodynamic and hydrodynamic conditions. Spatial differences in terrace morphology therefore may result in over- or underestimation of paleo relative sea levels and their associated uncertainties. To investigate this, we integrate high-precision field surveys from the island of Aruba (Leeward Antilles, Caribbean Sea) with a stratigraphic forward model (DionisosFlow®) to quantify the intra-island variability of the Quaternary coral reef sequence. We establish that a possible slight North-South tectonic tilt of the island may drive differences in the elevation of coral reef terraces and the number of emerged fossil coral reefs imprinted on the coastal landscape. However, terrace geometry is primarily defined by the basement slope and wave exposure. All together, our results show that even small-scale environmental and hydrodynamic variability can introduce meter-scale errors in sea-level reconstructions derived from coral reef terraces.

Plain Language Summary

Fossil coral reefs are valuable in reconstructing past sea-levels. However,

spatial differences in fossil coral reef morphology can lead to an over- or underestimation of past sea levels and their associated uncertainties. In this work, we integrate high-precision field surveys from the island of Aruba (Leeward Antilles, Caribbean Sea) with a model (DionisosFlow®) to investigate how fossil coral reef structure varries across the island. Our results show that, while a possible slight North-South tectonic tilt of the island may contribute to differences in the elevation and number of fossil coral reefs present, bedrock slope and wave exposure are the main factors shaping fossil coral reef geometry and ecology. These findings highlight the need to account for environmental context when using fossil coral reefs as sea-level proxies.

Key Points

12 stratigraphic forward models to unravel the morphological differences of Aruba's fossil coral reefs.

Antecedent bathymetry directly controls accreted reef geometry across glacial/interglacial cycles.

Wave exposure orchestrates resulting reef architecture, specifically community composition and facies framework.

1. Introduction

Geological reconstructions aimed at assessing patterns of sea-level change from previous warm periods provide invaluable insights into past sea-level changes (Dutton et al., 2015; Dyer et al., 2021). In tropical regions, paleo coral reefs provide several proxies that enable precise sea-level reconstructions (Dumitru et al., 2023; Rovere et al., 2023). This is due to the relatively narrow depth range of some coral species (e.g., Hibbert et al., 2016), the ease of dating fossil corals with both U-Series and radiocarbon techniques (e.g., Chutcharavan and Dutton, 2021), and the tendency of coral reefs to form terraces in close connection with sea level (Pedoja et al., 2018).

The genesis of a coral reef is strongly influenced by accommodation space, which is driven by the interplay between relative sea-level changes, reef growth rates, as well as antecedent topography (e.g., Camoin and Webster, 2015). Exposure to prevailing winds and related sea-states typically imprints an additional, distinctive, morphological and ecological fingerprint on coral reefs (differences between windward and leeward coasts; e.g., Speed and Cheng, 2021; Kennedy et al., 2012; Chauveau et al., 2025a).

As relative sea level falls, reefal limestones emerge and begin to erode, creating coral reef terraces (CRTs, Murray-Wallace and Woodroffe, 2014). CRTs are characterized by flat or slightly sloping surfaces, and are limited seaward by a distal edge, often delineated by a sea cliff of variable height, and landward by an inner edge, characterized by a break in slope (e.g., Chappell, 1974). Paleo sea-level reconstructions often use the CRT inner edge elevation as a sea-level proxy (Lajoie, 1986; Pirazzoli et al., 1991), or, if preserved, the elevation of the highest *in situ* corals (Rovere et al., 2016). However, the use of CRTs for paleo–sea-level estimation depends on assumptions about the formation factors outlined above. Most importantly, the pronounced structural heterogeneity of coral-dominated coastlines introduces previously underappreciated and significant limitations to these assumptions (e.g., Davis et al., 2021). One promising approach to mitigate this uncertainty is to employ process-based numerical models.

The use of numerical models simulating stratigraphic growth and demise of coral reefs to supplement field observations has been demonstrated as a valid approach across varying timescales and contextual complexities (e.g., Turcotte and Bernthal, 1984; Granjeon and Joseph, 1999; Warrlich et al., 2002; Webster et al., 2007; Koelling et al., 2009; Toomey et al., 2013; Montaggioni et al., 2015; Husson et al., 2018; Pastier et al., 2019; de Gelder et al., 2020; 2022; 2023; Boyden et al., 2023; Chauveau et al., 2024a; 2024b). However, most of these studies focused on disentangling the controlling mechanisms across 2D profiles perpendicular to the coastline or sequences that are situated along mainly homogenous coastlines. This begs the question: Can numerical models differentiate the effect of diverse geomorphic, hydrodynamic, and ecological conditions to better reflect the observed fossil record along heterogenous coasts? And therefore, can we better understand the limitations to using the CRT record for paleo sea level reconstruction?

In this study, we address these questions by investigating the environmental differences between the windward, leeward, and southern coasts of the island of Aruba (Caribbean Sea). The windward coast is characterized by high hydrodynamic energy, the leeward coast by relatively calm conditions, and the southern coast by energy levels slightly lower than those of the windward coast. By comparing these contrasting settings, we evaluate how spatial context influences potential sea-level and tectonic reconstructions. For example, does increasing wave exposure reduce the elevation and width of the CRTs, thereby affecting the reconstructions derived from them? We use field surveys to characterize the fossil reef record and its spatial variation. We then leverage Stratigraphic Forward Modelling using DionisosFlow® to attempt to numerically reproduce our field observations. This enables us to investigate how local variations in tectonics, hydrodynamics and coral community composition influence the preservation, morphology, and elevation of reef records over time and across intra-island spatial scales.

2. Study Area

The ABC islands (Aruba-Bonaire-Curaçao) are located on the Leeward Antilles ridge, which is the result of Cretaceous–Cenozoic tectonic interactions between the Caribbean and South American plates (Avé Lallemant, 1997; Beardsley and Avé Lallemant, 2007). The ABC islands are mainly composed of batholith, volcanic and sedimentary rocks with Neogene-Quaternary carbonate outcrops. The Neogene–Quaternary carbonate cover of ABC Islands includes Miocene limestones, with the majority of coastlines dominated by Pleistocene CRTs (de Buisonjé, 1974; Fouke et al., 1996; Fig. 1).

Three CRTs, increasing in height above sea level, have been described in Aruba, four on Bonaire and up to five on Curaçao (e.g., Alexander, 1961; Muhs et al., 2012; Lorscheid et al., 2017). The hybrid morphology of the ABC sequence, between a staircase morphology and stacked reef limestones indicates a slow vertical motion (around 0.05 mm a^{-1}) due to a combination of glacial isostatic adjustment (GIA) and tectonic uplift (Herweijer and Focke, 1978; Hippolyte & Mann, 2011; Muhs et al., 2012).

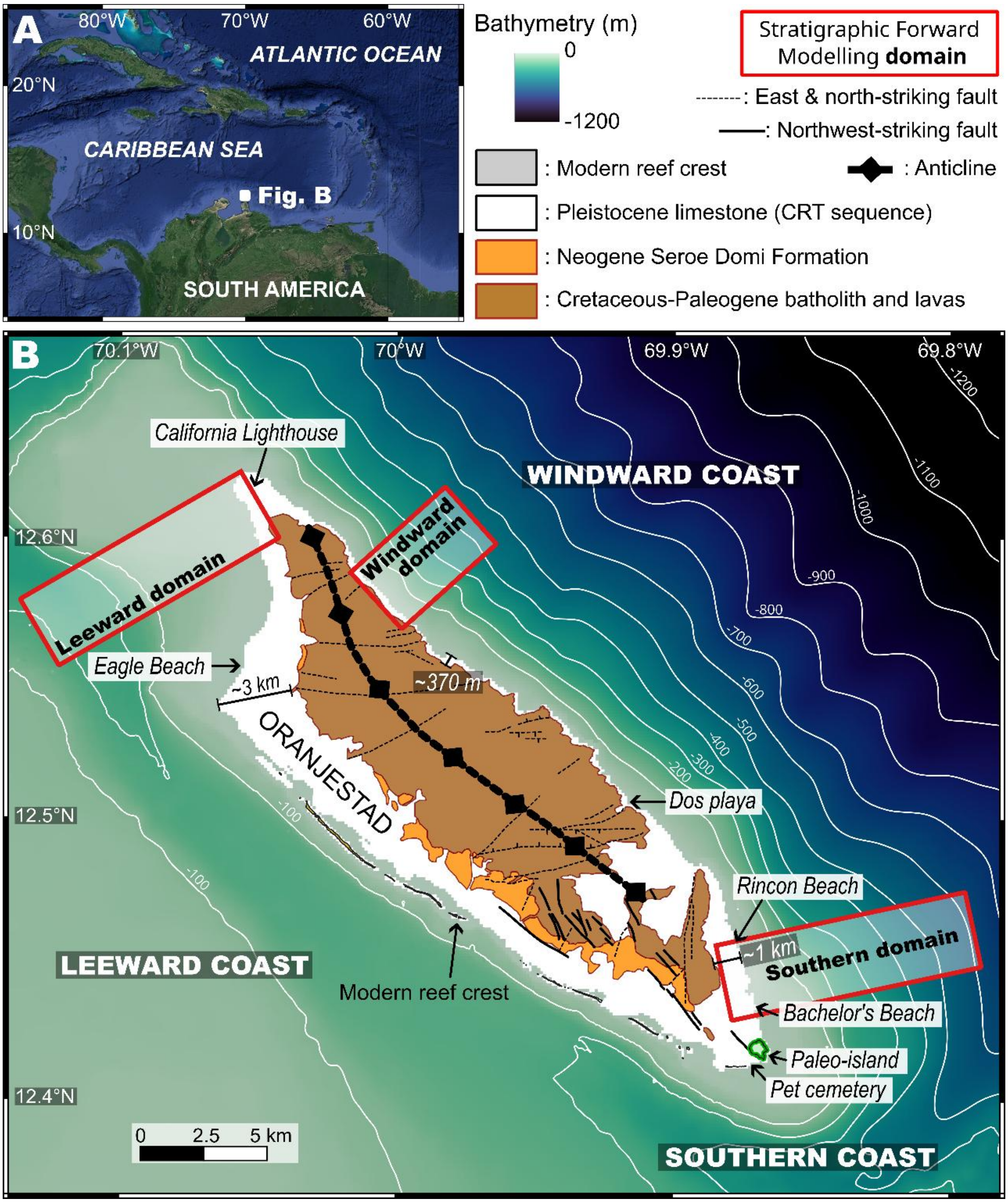

Figure 1. Map of **A)** the Caribbean Sea (from Google Earth, Data SIO, NOAA, U.S. Navy, NGA, GEBCO, Image Landsat/Copernicus) and **B)** Aruba, with model domains and names of sites mentioned in the text. Bathymetric data are the combination of the multibeam echo sounder used by the Dutch Ministry of Defense around the ABC islands (Dutch Caribbean Biodiversity Database, 2019) and the GEBCO dataset (10 m resolution). See Sect. 3.2.1. for more explanations. The Cretaceous-Paleogene and Neogene rocks were mapped using the work of White et al., (1999) and Hippolyte & Mann (2011). The faults and the fold were mapped using the work of Hippolyte & Mann (2011).

The lowermost CRT of the ABC islands (CRT 1, ranging in elevation between 0 and 15 m above sea level) is associated with very well-preserved tidal notches (Lorscheid et al., 2017) and fossil corals (e.g., Meyer et al., 2003). On Curaçao, CRT 1 is predominately composed of the so-called Hato Unit (Marine Isotope Stage, MIS, 5e), overlaying a thin exposure of the so-called Cortalein Unit (MIS 7) (Muhs et al., 2012). On Bonaire, CRT 1 has been dated to MIS 5e (Obert et al., 2016; Lorscheid et al., 2017). Although no corals have been dated on Aruba, given its proximity to Curaçao and Bonaire and its similar geodynamic and biostratigraphic context, the lowermost CRT on Aruba can also be confidently ascribed to MIS 5e. While the two CRTs above CRT 1 are interpreted to be older (e.g., Muhs et al., 2012), no age or MIS has been established with certainty.

3. Methodology

3.1. Field surveys

Surveys took place during a field campaign in May 2023, spanning the Pleistocene CRT sequence surrounding the island of Aruba at three distinct domains: leeward, windward, and southern coasts (Fig. 1B). We studied a total of 13 sites: five sites for the leeward and windward domains and three for the south domain. Topographic transects were surveyed at each site using an EMLID RS2+ differential GNSS (dGNSS) receiver, following a Post-Processed Kinematic (PPK) workflow. Archived RINEX base station data from the nearby NOAA Continuously Operating Reference Stations (CORS) CN19 was downloaded from the EarthScope Consortium (UNAVCO, https://data.unavco.org/archive/gnss/logs/cn19log.txt). Once post-processing in Emlid Studio (EMLID, 2024) was carried out, the collected ellipsoidal elevations were then converted into Earth Gravitational Models (EGM) 2008 geodetic elevations (Pavlis et al., 2012) and the final root mean square (RMS) values (95% confidence interval) were calculated as the RMS of the EGM08 conversion RMS (0.0022 m) and the Ellipsoid RMS output from Emlid Studio. All processed survey data can be found in the Supplementary Material (Supplementary-Information-dGNSS-data).

We also performed three land-based Structure from Motion/Multi-View Stereo (SfM/MVS) surveys of reef facies outcropping within sections of the CRTs along the windward and southern coasts to extract their morphological features. SfM/MVS surveys were not possible on the leeward coast due to extensive urban development. Approximately 750 photos were acquired at each site using a 20.1-megapixel Sony DSC-RX100M3 camera (8.8 mm focal length and resolution of 5472 × 3648 pixels) mounted on a 3 m collapsible pole. Coded ground control points (GCPs) were measured with dGNSS and processed following the same PPK workflow described above. Photos and GCPs were then processed in Agisoft Metashape Professional (v.2.1.0 build 17532) to build digital twins of each outcrop and georeferenced digital terrain models (DTMs). Finally, to obtain a detailed understanding of the CRT succession at each site and provide appropriate inputs to the stratigraphic forward model workflow described below, we compiled detailed biostratigraphic sketches of each outcrop. Each digital twin was then annotated to provide model inputs and to enable semi-quantitative comparisons between the paleo- and modelled-records.

3.2. Stratigraphic forward modelling

In this study, we used the 3D stratigraphic forward model DionisosFlow® from *IFP Energies nouvelles* and Beicip-Franlab to simulate the CRT sequence along the coast of Aruba and compare the modelling outputs with the field observations at three locations: leeward, windward and southern domains, Fig. 1 and Fig. 2). DionisosFlow® was originally developed to explore the fundamental controls on the stratigraphic architecture of both carbonate and siliciclastic systems at basin scale (10–100 km), across geological timescales spanning 0.01 to 100 Ma (Granjeon & Joseph, 1999; Rabineau et al., 2005; Granjeon et al., 2005; Burgess & Wright, 2003). More recently, it has been adapted to simulate Holocene reef systems enabling high-resolution reconstructions of depositional geometries over finer temporal and spatial scales (Seard et al., 2013). Therefore, DionisosFlow® simulates sediment production and distribution across a range of depositional environments, including terrigenous and carbonate systems, from coastal zones to platforms, slopes, and deep basins (Granjeon & Joseph, 1999; Granjeon et al., 2005; Rabineau et al., 2005; Burgess et al., 2006; Andres et al., 2008; Bassant & Harris, 2008; Claps et al., 2009; Williams et al., 2011; Seard et al., 2013; Boyden et al., 2023).

The modelled morphometric values and virtual reef facies are extracted from the domains defined below (Section 3.2.1., and red squares in Figures 1 & 2), whereas the morphometric measured values (derived from TanDEM-

X and dGNSS transect data) and observed field data encompass almost the entire leeward, windward, and southern coastlines. In addition to the windward and leeward coasts, we included the island's southern coast in our analysis due to the presence of a unique sequence of three CRTs, a geomorphic feature not observed elsewhere on the island. The leeward domain is defined here as the island's northwestern sector, representing the only remaining segment of the leeward coast that retains its natural state, with all other sections having been extensively modified by anthropogenic activity. DionisosFlow® uses several distinct parametric components which are detailed below.

3.2.1. Topography and bathymetry

The emerged (fossil) and submerged (living) coral reefs of Aruba have not been subject of coring or seismic campaigns, and no high-resolution nearshore bathymetry and definition of subsurface horizons exist for this area. To overcome this issue, we adopted two different approaches, that translate into different modelling scenarios.

In the first scenario, we created a bathymetry following the assumption that the coastal geometry at the start of our simulations was approximately the same as it is today. To do this we down-sampled and combined previously published nearshore multibeam bathymetry data (Dutch Ministry of Defense, Dutch Caribbean Biodiversity Database, 2019) with a GEBCO dataset around Aruba (Figs. 1; 2).

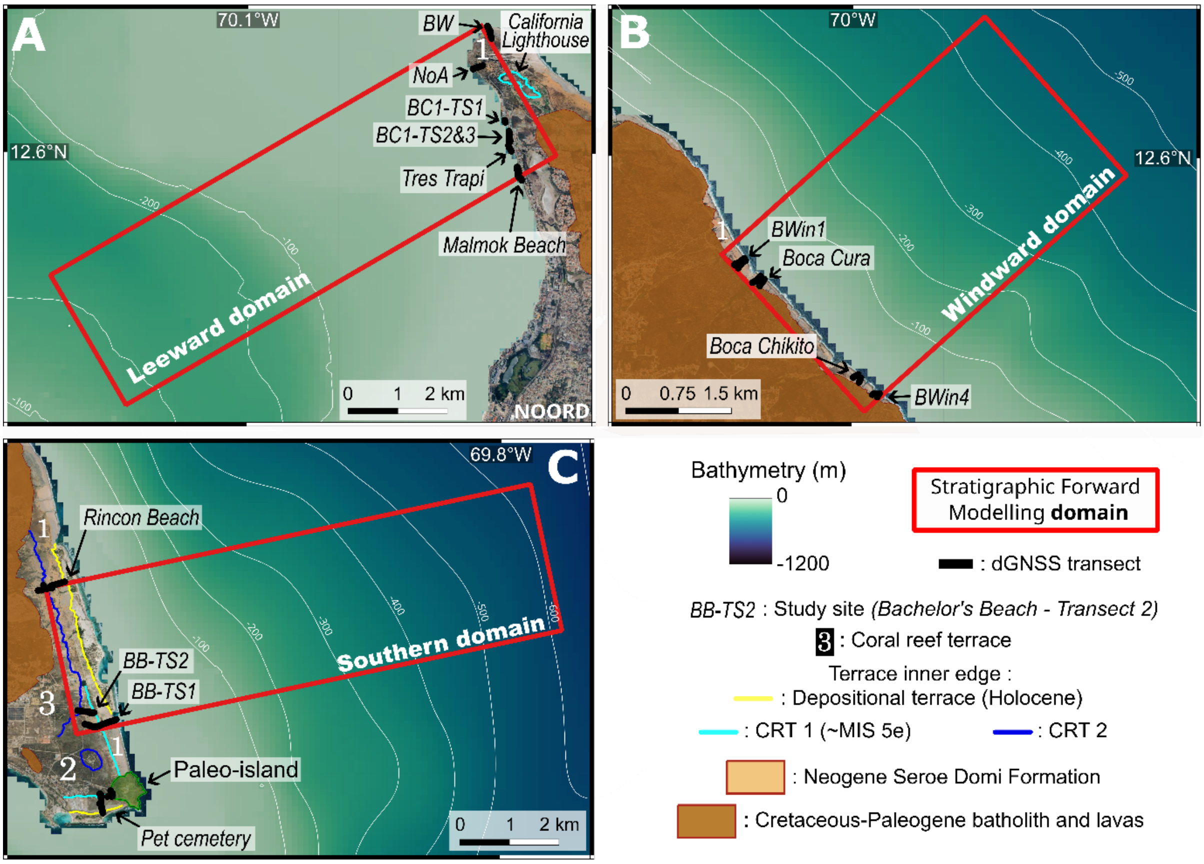

Figure 2. Map of the **A)** leeward, **B)** windward, and **C)** southern domains. dGNSS transects are marked with black lines. The acronyms correspond to the different sites studied here and are defined as follows: BW: Boca Westpunt; NoA: North of Arashi; BC: Boca Catalina; BWin1: Boca Windward 1; BWin4: Boca Windward 4; BB: Bachelor's Beach. BWin1 and BWin4 have no official names, so we have simply given them a number, with 1 for the most northerly Boca and 4 for the fourth Boca from the north. Satellite images come from Google Earth (ESRI, Data SIO, NOAA, U.S. Navy, NGA, GEBCO, Aribus, TerraMetrics, Data LDEO-Columbia, NSF). The inner edges of the terraces were mapped using the dGNSS transects, the Digital Elevation Model TanDEM-X from the German Aerospace Center (12 m resolution) and Google Earth. Bathymetric data are the combination of the multibeam echo sounder used by the Dutch Ministry of Defense around the ABC islands (Dutch Caribbean Biodiversity Database, 2019) and the GEBCO dataset (10 m resolution). See Sect. 3.2.1. for more explanations.

In the second scenario, we generated a linear slope that mimics the apparent slope of the volcanic basement of the island, calculated from the elevation of the highest and lowest contacts observed and measured between the Pleistocene limestone and the Cretaceous-Paleogene rocks. In the windward and leeward domains this is 19.0% and 3.1%, respectively. Due to the intense anthropogenic alteration of the leeward coast, no potential contact could be observed between the Pleistocene limestones and the Neogene Seroe Domi Formation. For the southern part, as no basement rocks are visible, we calculated a representative slope from the maximum elevations and distance from the coastline of the dGNSS transects at 3.5% (Table 1). With our modelling domains extending over 3 x 5 km for the windward coast and 3 x 10 km for the leeward and southern coasts, the slope values reach depths greater than the amplitude of the glacio-eustatic cycles (i.e., ~120 m), and prevent an unrealistic simulation that is completely filled with sediment and carbonate deposition.

These two scenarios implemented in the 3D DionisosFlow® model also enable an assessment of how complex bathymetry influences coral reef growth, in comparison to a simplified linear slope. Under both scenarios described above, the windward, leeward, and southern domains were rotated from the horizontal by respectively -42°, 60°, and -12°. In this way, the shoreline becomes roughly horizontal through the gridded domain and therefore intra-grid incident angles during wave propagation calculations are minimized (e.g., Roelvink et al., 2009). Finally, the model grid resolution is set at 50 x 50 m, which allows for a reasonable approximation of the nearshore wave environment (Table 1, Boyden et al., 2023).

Table 1. DionisosFlow® model domain grid and bathymetric horizon parameters used.

Domain (coastal side)	Coordinates (WGS 84)	Azimuth (°)	Grid extent (km)	Linear basement	Maximum depth (m)	Grid resolution (m)	Cell count

	X_0	Y_0		Length	Width	slope (°)	Linear	Current Bathy.	D_x, D_y	N_x, N_y
Leeward	-70.136°E	12.578 °N	60	10	3	3.1	310	250	50, 50	60, 200
Windward	-69.998°E	12.567 °N	-42	5	3	19	950	450	50, 50	60, 100
Southern	-69.879°E	12.429 °N	-12	10	3	3.5	350	400	50, 50	60, 200

3.2.2. Sediment classes

The DionisosFlow® model implements user-defined sediment classes to resolve complex reef environments. Here, we defined four main reef framework contributors: *Acropora cervicornis*, *Acropora palmata*, *Diploria* spp., and *Orbicella* spp.*,* all of which can be found both in the modern and exposed paleo reefs of the ABC Islands (e.g., Alexander 1961; Van Duyl, 1985; Pandolfi and Jackson, 2001). Additionally, generic carbonate sand and carbonate mud classes along with a volcanic "Basement" class are also defined.

Each of the seven classes is then parameterized by the type of sediment (carbonate, clastic, evaporate, etc.), grain size, solid density, and burial compaction law (observed of mechanical). In this case, the grain size chosen for corals corresponds to the average size of a solitary colony of each respective species (Table 2). The initial sediment class is set as the Cretaceous volcanic "basement" over the entire model domain, with an initial thickness of 50 m to account for any subsequent erosion of this layer. While siliciclastic sediment and fluvial input can be added to the model, neither are included as the coast of Aruba is only punctuated by small ephemeral fluvial incisions (locally called *bocas*), for which sediment transport is assumed to be negligible. The sediment classes defined in our model (and their properties) are summarized in Table 2.

Table 2. Sediment classes, including grain size and solid density, and wave energy range for each sediment class used within DionisosFlow®.

Sediment class	Grain size (mm)	Solid density (kg m^{-3})	Wave energy range (kW m^{-1})
Acropora cervicornis	50	2710	5 - max
Acropora palmata	300		10 - max
Diploria spp.	500		min - 5
Orbicella spp.	300		min - 5
Carbonate mud	0.004		min - 1
Carbonate sand	1		min - 5
Volcanic rock	1000	2500	

The overall reef architecture, and the ensuing framestone, lessens the changes in pore space at shallower burial depths, and therefore we treat the reef 'sediment' compaction as negligible, whereas resulting sand and debris facies are governed by a simplified mechanical compaction that is linear to depth. Potential increases in hinterland precipitation and associated clastic sediment influx during glacial periods are acknowledged but lie outside the scope of this study. While dewatering of compacting siliciclastic sediments can substantially influence basin-scale water budgets (Revil et al., 2002), carbonate systems are characterized by highly heterogeneous porosity that undergoes significant modification during early burial (i.e., diagenesis; Lee et al., 2021), rendering their fluid dynamics more complex and less predictable.

DionisosFlow® automatically calculates the slope-driven and water-driven diffusion coefficients along the depositional profile from the grain size distribution. These coefficients are derived from an empirical database established by Beicip-Franlab, built from the calibration of numerous basin-scale studies worldwide. This database links sediment transport efficiency to grain size and depositional context, allowing realistic estimation of diffusion parameters without manual tuning. At regional spatial scales and over geological timescales, local and short-term sediment transport processes can be upscaled to yield a linear diffusive transport law:

$$Q_s = S*K_{slope} + S*Q*K_{water} \quad (1)$$

where Q denotes sediment flow ($m^2\ s^{-1}$), K_{slope} is the slope-driven diffusion coefficient ($km^2\ ka^{-1}$), K_{water} is the water-driven diffusion coefficient ($km^2\ ka^{-1}$), Q is the surface of the basin, and S is the elevation gradient (basin slope). At each spatial location (corresponding to the grid resolution of 50 m), sediment flux is thereby controlled by two primary variables: the local slope, which dictates the gravitational potential driving fluid movement, and the water flow, which modulates sediment transport capacity. The diffusion coefficient mediates the relationship between slope and water flux, encapsulating the mean transport efficiency characteristic of a given depositional setting. It is not constant but evolves with the prevailing depositional dynamics—whether fluvial, tidal, or wave-dominated—thus embedding the influence of environmental forcing into large-scale sediment transport behavior (Granjeon, 1997; Granjeon & Joseph, 1999).

3.2.3. Carbonate production

In DionisosFlow®, the spatial and temporal variability of carbonate production due to water temperature, turbidity, wave energy, and water depth (e.g., Montaggioni and Braithwaite, 2009), is solved by first defining each carbonate producer among the sediment classes from Sect. 3.2.2. (i.e., all sediment classes except volcanic rock, Table 2). Then, an additional user-defined production-versus-depth value is added to each carbonate sediment class, which represents the non-linear relationship between carbonate growth rate and depth (Fig. 3).

For the purposes of this study, we apply published growth rates and living depth curves for each coral-based facies (i.e., *Acropora* spp.*, Diploria* spp. and *Orbicella spp.*, Dullo, 2005 and Hibbert et al., 2016), as well as carbonate sand and mud curves come from Burgess and Pollitt (2012) (Fig. 3). Unlike Montaggioni et al. (2015), who experimented with varying growth rates through time validated by borehole data on Mururoa (Central Pacific Ocean), we held all carbonate production temporally constant. This is done to minimize assumptions as seismic and borehole data for Aruba is lacking.

Therefore, our simulations are run with constant maximum growth rates from the literature mentioned above, i.e., 1.8 x 10^5 m Ma^{-1} for *A. cervicornis*, 9 x 10^4 m Ma^{-1} for *A. palmata*, 7800 m Ma^{-1} for *Orbicella* spp., 3500 m Ma^{-1} for *Diploria* spp., and 1000 m Ma^{-1} for carbonate sand and carbonate mud throughout the model run (Fig. 3). The growth potential of reefs and carbonate platforms depends on the maximum growth rate of frame-building organisms (Dullo, 2005). We therefore use the maximum coral growth rate to examine the theoretical upper limit of coral cover, providing insight into aspects of reef development that lower growth rates would not capture.

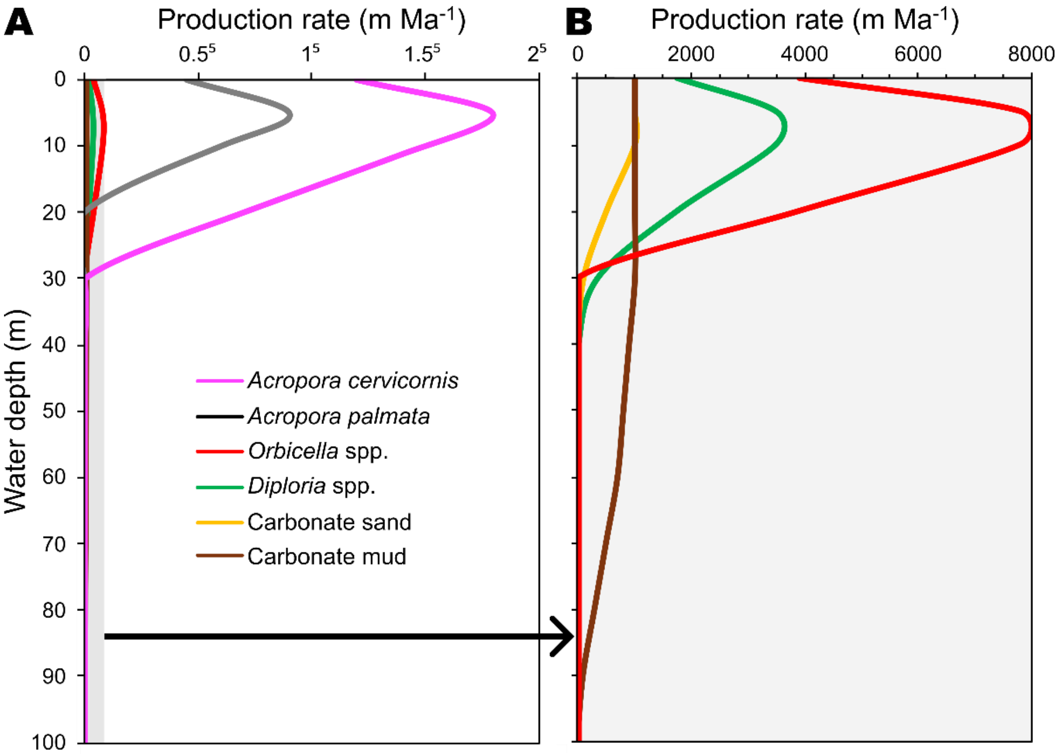

Figure 3. Production rate (m Ma^{-1}) as a function of water depth for each sediment class included in the DionisosFlow® model. As the growth rates of *Acropora* spp. are tens of times higher than the growth rates of the other species, we separate the curves as follows: **A)** with and **B)** without *Acropora* spp. (i.e., grey zone).

The respective wave energy range in which each corals facies can grow is based on the results of previous studies (Seard et al., 2013; Boyden et al., 2023; Table 2). *Diploria* spp. and *Orbicella* spp. are massive corals, and *Acropora* spp. branching corals. The latter is then further differentiated between *A. cervicornis* and *A. palmata* because **1)** *A. cervicornis* lives in more protected environments (fore- and back-reef settings) than *A. palmata* (reef-crest and upper-reef zones, Montaggioni and Braithwaite, 2009), and **2)** *A. cervicornis* has a greater growth depth range than *A. palmata* (Fig. 3; Hibbert et al., 2016).

3.2.4. Hydrodynamics

The dominant wave direction and magnitude have a significant influence on both shoreline geometry and the ability of coral colonies to flourish (Gischler et al., 2019). In DionisosFlow®, wave energy and refraction with respect to bathymetric depth are evaluated using Snell s law (e.g., Holthuijsen, 2010). As no direct measurements of wave height during MIS 5e exist, we apply the assumption that the modern average wave climate provides an appropriate approximation. Therefore, the mean significant wave height (Hs) and direction were extracted for each corresponding model domain from the Centre for Australian Weather and Climate Research (CAWCR) global hindcast raster and are summarized in Table 3 (Durrant et al., 2013). The CAWCR is based on WaveWatch III wave model outputs from 1979–2010 on a 0.4 x 0.4-degree global grid. Additionally, storms, and specifically tropical cyclones, play a crucial role in coral reef development and colony long-term stability (Gardner et al., 2005). To approximate these impacts, the respective maximum significant wave heights and directions from the CAWCR model were also extracted and added to each model at 10% yearly occurrence intervals (Table 3).

Table 3. Model hydrodynamic boundary conditions.

	Domain		
Average conditions	Windward	Leeward	Southern
Wave base (m)	6.34	5.51	6.3
Propagation azimuth (°)	270	0	270
Wave energy flux (kW m^{-1})	15.82	11.63	15.6
Wave height (m)	2.28	1.98	2.26
Storm			
Wave base (m)	22	14.51	20.21
Propagation azimuth (°)	270	0	270
Wave energy flux (kW m^{-1})	28.49	10.43	23.13
Wave height (m)	7.9	5.21	7.25

A significant limitation of DionisosFlow® is its omission of wave-related erosion component (i.e., allowing horizontal erosion of emerged geological units). This type of erosion plays a critical role in the CRT morphogenesis (e.g., Chauveau et al., 2021).

3.2.5. Sediment weathering

In our models, three forms of weathering are taken into account: **1)** maximum weathering rate, **2)** dissolution rate, and **3)** transformation rate. Compared to previous studies conducted in significantly wetter climates, like Mururoa Island (Central Pacific Ocean) where Montaggioni et al. (2015) used a maximum weathering rate of 250 m Ma^{-1} driven by a mean annual rainfall rate of 1350 mm a^{-1}, Aruba receives a relatively low annual rainfall rate (~400 mm a^{-1}; www.aruba.com: Last visit: 13th November 2024). Therefore, we chose a constant weathering rate of 100 m Ma^{-1} as previously used in a similar coastal environment on Madagascar (i.e., Lembetabe, Boyden et al., 2023), and affected by a similar annual rainfall rate (386 mm/yr in Toliara, about 160 km north of Lembetabe, along the same coast, Dewar & Richard, 2007). To simplify the computational load, the dissolution rate is treated as constant and incorporated within our maximum weathering erosion rate. Finally, the transformation rate, which allows for the conversion of mass from deposited carbonate into carbonate sands and muds, is set to a constant 50 m Ma^{-1} rate for each sediment class, except for carbonate sand and carbonate mud (Boyden et al., 2023).

3.2.6. Relative sea level

Beyond ice sheet mass balance, post-depositional processes can significantly affect relative sea level (RSL) through glacial/interglacial cycles. Generally, this includes processes such as GIA (Mitrovica and Milne, 2003), dynamic topography (e.g., Austermann et al., 2017), tectonics (e.g., Pedoja et al., 2011), and other vertical land motion processes. In Aruba, the combined effects of GIA and tectonic uplift have likely contributed to the post-depositional vertical displacement of Pleistocene fossil reefs, with estimates indicating vertical land motions of ~0.05 mm a^{-1} (Herweijer and Focke, 1978; Hippolyte & Mann, 2011; Muhs et al., 2012). As a result, the present-day elevations of CRTs cannot be interpreted solely as indicators of past global mean sea level (GMSL) but instead reflect the combined imprint of multiple vertical deformation processes superimposed on GMSL oscillations.

As relative sea-level input to our model, we used the GMSL curve of Waelbroeck et al. (2002), except for MIS 5e, where we imposed a relative sea-level history derived from the GIA models developed in Barnett et al. (2023), using the best-performing parameters retrieved in the Bahamas by Dyer et al. (2021) (Fig. 4). This highest ranked scenario uses a 96 km lithosphere thickness, an upper viscosity of 5 x 10^{21} Pa s^{-1}, a lower mantle viscosity of 40 x 10^{21} Pa s^{-1}, and a relatively moderate thickness (66 m) for the Laurentide Ice Sheet that uses a slow timing for the MIS 6 deglaciation. Then, to the model-calculated GIA, we added the maximum sea level calculated by Dyer et al. (2021) (i.e., 5.3 m above present mean sea level from 130 ka to 116 ka). This approach allows us to prescribe a MIS 5e sea-level history that is consistent with both ice-sheet evolution and Earth-structure parameters.

Based on this sea-level history, two assumptions are then made: with and without an uplift rate of 0.5 mm a^{-1} directly integrated into the input RSL curve (Fig. 4). The uplift rate value is based on previous estimates (Section 2; Herweijer and Focke, 1978, Schubert and Szabo, 1978; Hippolyte & Mann, 2011; Muhs et al., 2012). Using these two RSL signals is essential for assessing the extent to which local vertical land-motion processes may have modified the GMSL signal recorded in the CRT sequence. The time step of the RSL curve as well as the model is 1 ka (Fig. 4).

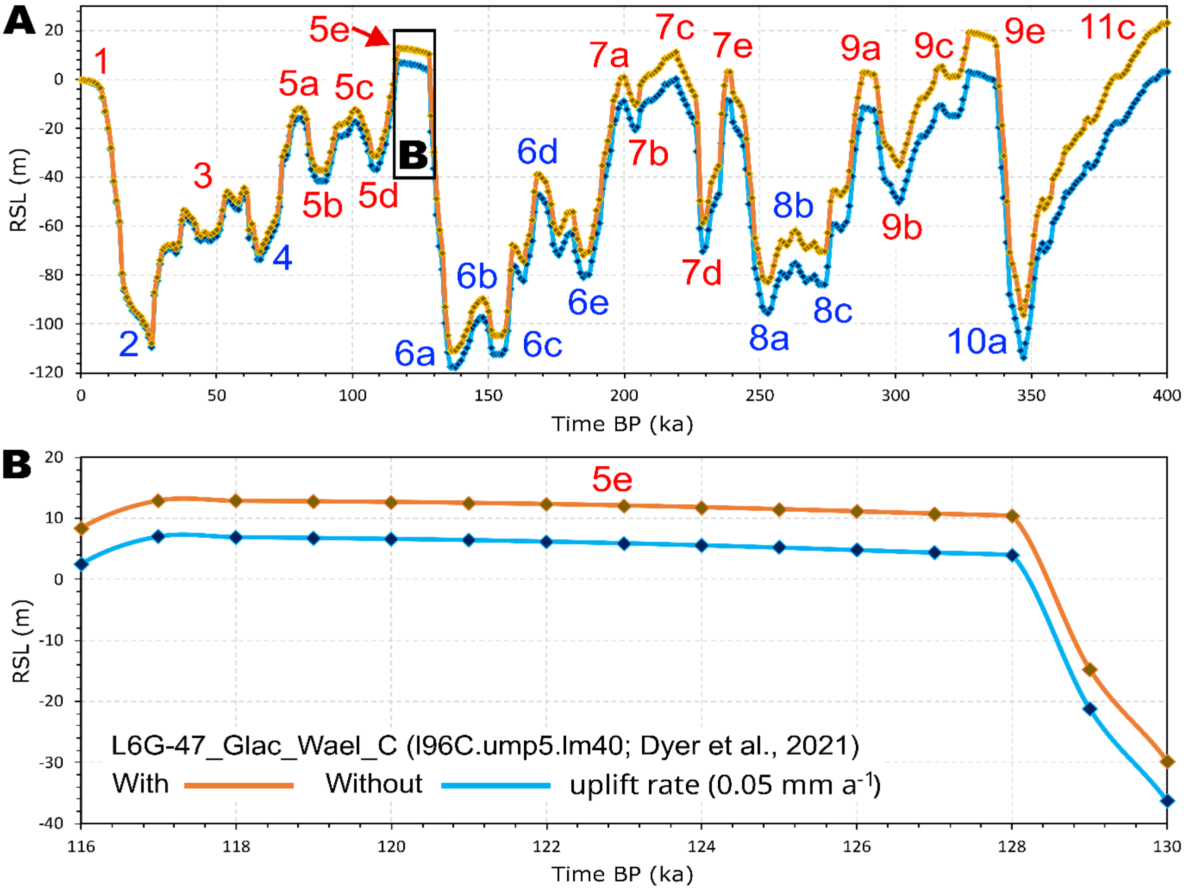

Figure 4. Input RSL curve. In light blue, the RSL curve from Dyer et al. (2021). In orange, the same curve with an integrated uplift rate of 0.05 mm a^{-1}. Each diamond corresponds to 1 ka steps as model input. MIS nomenclature (numbers and letters) is from Railsback et al. (2015). The MIS in red are the interglacial stages and in blue the glacial stages. Only clearly distinct MIS (in terms of sea level amplitude) on these curves are written and considered in this study.

Overall, considering all the different modelling scenarios described above, we used 12 different model runs, four for each domain (i.e., scenarios with a linear slope or with the current bathymetry, each affected or not by uplift, Table 4).

Table 4. Different scenario within DionisosFlow®.

Domain (coastal side)	Bathymetry	Land motion	
		No Uplift (NU)	Uplift (0.05 mm a^{-1}) (U)
Leeward (L)	Current Bathymetry (CB)	L-CB-NU	L-CB-U
	Linear Slope (LS)	L-LS-NU	L-LS-U
Windward (W)	Current Bathymetry (CB)	W-CB-NU	W-CB-U
	Linear Slope (LS)	W-LS-NU	W-LS-U
Southern (S)	Current Bathymetry (CB)	S-CB-NU	S-CB-U
	Linear Slope (LS)	S-LS-NU	S-LS-U

3.2.7. Facies definition

During post-processing, seven facies were defined following the coral distribution scheme laid out by Montaggioni et al. (2015) for reef-dominated coasts as well as model-specific environmental constraints from Seard et al. (2013). Moving landward over the reef, we define the following facies: **1)** fore reef, **2)** reef crest, **3)** lagoon, **4)** back reef, **5)** beach, **6)** basement, and **7)** undefined. The relationships between sediments and environmental controls within the model output are summarized in Table 5. Each facies is a combination of one or more of the sediment classes described before (Sect. 3.2.2.) and deposition depth.

Table 5. Facies definition within DionisosFlow®. Adapted from Seard et al. (2013), Montaggioni et al. (2015), and Boyden et al., (2023). The basement facies is not shown because it contains exclusively volcanic rock and is older than the simulation presented below. When "Min-Max" is specified, this means that the sediment class must be present in the facies, regardless of its percentage. Negative bathymetry (i.e., for the beach facies) means elevation above present mean sea level (apmsl).

			Facies				
			Fore reef	Reef crest	Lagoon	Back reef	Beach
Sediment classes (%)	*Orbicella spp.*	min	/	Min	Min	/	/
		max		Max	Max		
	Diploria spp.	min	/	Min	Min	/	/
		max		Max	Max		
	Acropora palmata	min	/	Min	/	Min	/
		max		Max		Max	
	Acropora cervicornis	min	Min	/	Min	Min	/
		max	Max		Max	Max	
	Carbonate sand	min	/	/	/	Min	Min
		max				Max	Max

Carbonate mud	min	/	/	Min	Min	Min
	max			Max	Max	Max
Wave energy (kW m^{-1})	min	Min	Min	Min	Min	Min
	max	15	Max	5	10	5
Bathymetry (m)	min	10	0	0	-1	-10
	max	120	10	30	5	-1

3.2.8. Well logs

In order to evaluate the differences in modelled facies between each scenario, synthetic well logs reflecting the declared facies were created directly in DionisosFlow® (Table 6). These were extracted at the virtual morphological locations closest to those surveyed in the field: i.e., the distal edge of CRT 1 for the leeward and southern domains and the middle of CRT 1 for the windward domain.

Table 6. Location of the well logs. Measurements of Z (relative to the present mean sea level) and distance from the coastline were made with DionisosFlow®.

Domain	Scenario	Morphological location	Coordinates (WGS 84)		Z top	Distance from the coastline
			X_0	Y_0	m	m
Leeward	CB-NU	Distal edge of CRT 1	-70.101°E	12.581° N	-5.0	804
	CB-U		-70.106°E	12.581° N	10.0	734
	LS-NU		-70.100°E	12.587° N	-3.5	487
	LS-U		-70.100°E	12.585° N	10.2	757

Windward	CB-NU	Middle of CRT 1	-69.993°E	12.587° N	-3.0	409
	CB-U		-69.993°E	12.589° N	11.0	515
	LS-NU		-70.002°E	12.583° N	-2.3	307
	LS-U		-70.000°E	12.583° N	12.4	278
Southern	CB-NU	Distal edge of CRT 1	-69.852°E	12.449° N	-2.2	523
	CB-U		-69.850°E	12.450° N	12.1	723
	LS-NU		-69.838°E	12.453° N	-3.0	595
	LS-U		-69.835°E	12.453° N	12.0	758

4. Results

4.1. Morphology of fossil coral reefs

Our field observations and the topographical data acquired show morphological differences among the leeward, windward and southern coasts of Aruba.

Representing the distal edge of the terrace sequence, the dGNSS topographic profiles of the leeward coast (Figs. 2A; 5A) have a generally lower elevation than those on the windward (Figs. 2B; 5C) and southern coasts (Figs. 2C; 5D). The maximum average measured elevation of CRT 1 of the leeward coast transects is 3.1 ±1.5 m above present mean sea level (apmsl) and increases to 6.7 ±1.5 m on the windward coast and 11.2 ±0.2 m on the southern coast. The number of CRTs intercepted by each dGNSS transect increases towards the south, from a single terrace (on the leeward and windward coast, except for the California Lighthouse site, Fig. 1) to two

CRTs south of Dos Playa and then three from Rincon Beach to Bachelor's Beach (Figs. 2C; 5D).

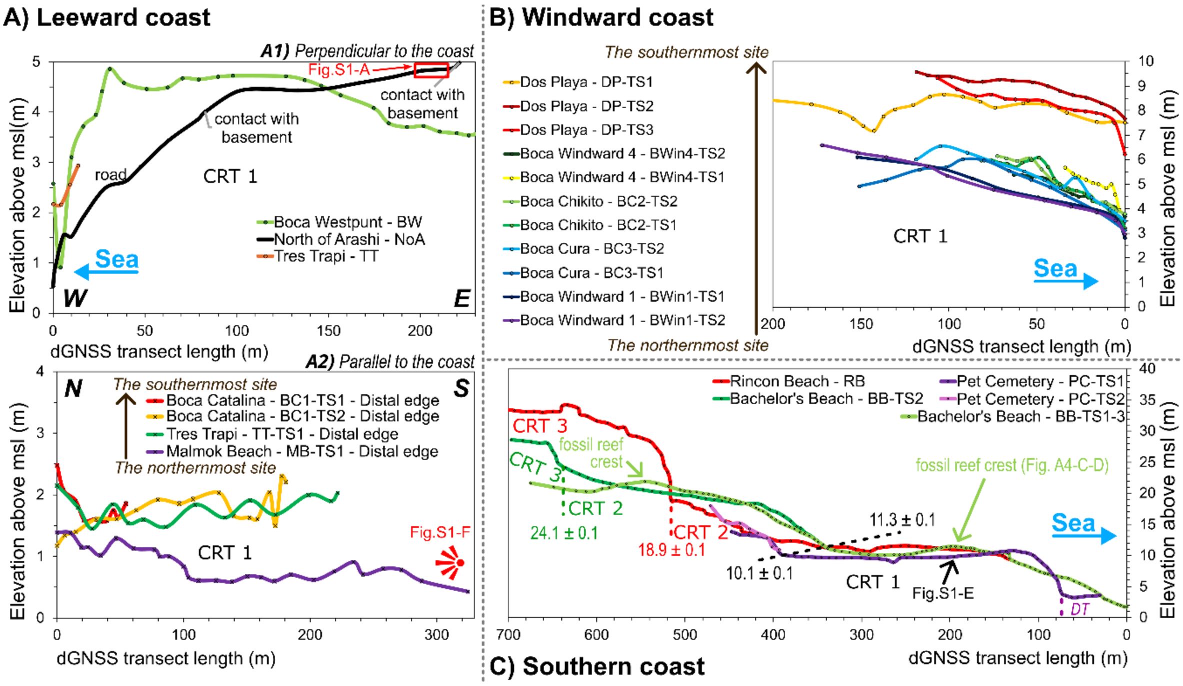

Figure 5. dGNSS transects of the **A)** leeward (perpendicular and parallel to the coast), **B)** windward, and **C)** southern coasts of Aruba. All the topographic data are relative to the mean sea level (msl). “TS” means “transect”. “DT” (Fig. C) corresponds to "Depositional Terrace".

The reef composing the terrace is relatively thin on the leeward coast, with a reef veneer a few decimeters thick in contact with the volcanic rocks (Figs. 5A; S1). CRT 1 on the windward coast is a few meters thick, with corals that have grown directly on the basement (Fig. S1-B-C-D). We did not observe any contact between the CRT and the basement on the southern coast, but we observed a CRT several meters thick in sinkholes at the “Pet Cemetery” site (Fig. S1-E). Thus, the fossil reefs are thickest in the south and thinnest on the leeward coast.

We highlight that, perpendicular to the coast, the CRT sequence is wider on the leeward than on the windward coast (Figs. 1; 6A). However, it is difficult to measure the exact width of the sequence on the leeward coast because of anthropic development. Previous studies have suggested that it is several kilometers wide (e.g., White et al., 1999; Hippolyte & Mann, 2011), making this the coast where the sequence is the widest among those investigated in this work.

4.2. Modelled morphology of fossil coral reefs

The model outputs show the same morphological characteristics observed and measured in the field. With an average of 6.9 km, the modelled CRT sequence for the leeward domain is wider than those on the windward and southern domains (1.9 km and 5.0 km respectively, Fig. 6A). However, despite a strong linear correlation between the modelled and measured sequence widths ($R^2 = 0.8$), the modelled CRTs are on average four times greater in width than the respective observed CRTs (Fig. 6A).

The maximum modelled elevation of the sequence is higher in the leeward domain (average of 14.1 m) than in the other domains (10.2 and 13.3 m for the windward and southern domains respectively; Fig. 6B). For which concerns the elevation of CRT 1, the modelled values are more homogeneous, with average values between 8.0 m (windward domain) and 9.8 m apmsl (leeward domain, Fig. 6C). The modelled and measured elevations of CRT 1 demonstrate a reasonable degree of agreement, with the exception of the leeward domain where dGNSS measurements represent the distal edge and not the inner margin.

In all domains, there is very little difference in maximum elevation (measured sequence and CRT 1) between the scenarios without uplift (i.e., Fig. 6B). On the other hand, a greater difference emerges between the domains when the uplift is taken into account. A maximum of 22.1 m is reached for the leeward domain, 19.5 and 16.4 m for the southern and the windward domains, respectively. All these values are achieved with the uplifted current bathymetry scenarios (i.e., CB–U scenario, Fig. 6B). Furthermore, when comparing the effects of basement geometry, a difference of several meters occurs between the uplifted linear and uplifted current bathymetry scenarios (e.g., 4.7 m for the windward domain). Conversely, this difference is not observed for the scenarios without uplift (1.4 m between the non-uplifted linear and current bathymetry scenarios for the windward domain). Therefore, vertical land movements would tend to accentuate the influence of initial bathymetry geometry on new reef construction, with higher elevation differences between the scenarios as the uplift rate increases.

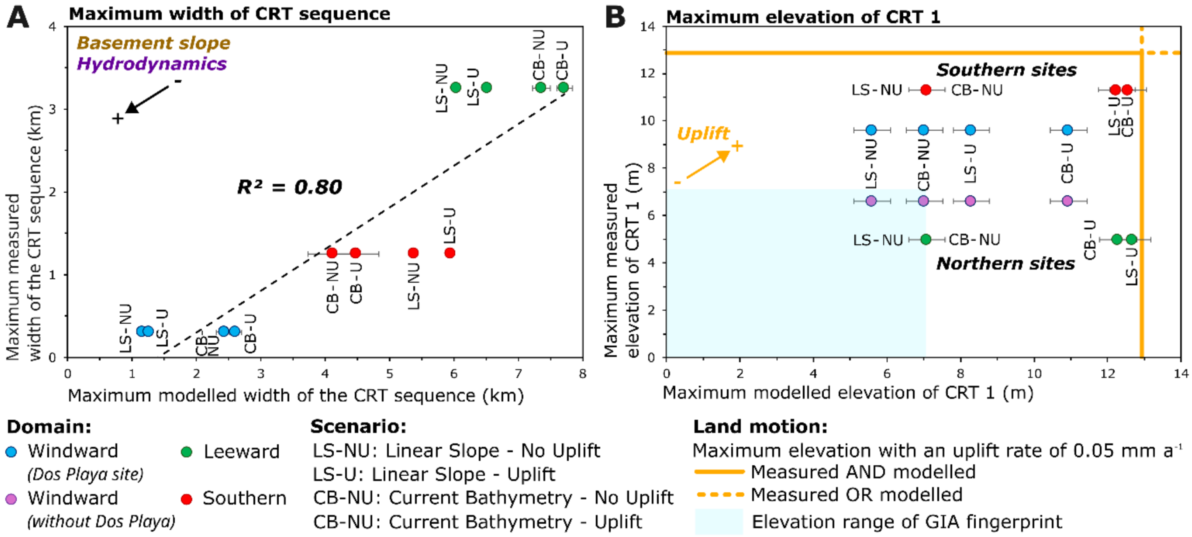

Figure 6. Morphometry of the measured and modelled CRTs as a function of the different scenarios for each domain. **A)** Width of the CRT sequence. **B)** Maximum elevation of CRT 1. The modelled morphometric values were measured directly in the DionisosFlow® software, while the others were measured using TanDEM-X for width and dGNSS transects for elevation. The modelled morphometric values are restricted to the domains defined in Section 3.2. (red squares in Figures 1 & 2), whereas the measured values (derived from TanDEM-X and dGNSS transect data) encompass the entire leeward, windward, and southern coastlines. The uncertainties on the modelled width values correspond to the minimum and maximum limits measured. We assign a value of ±0.5 m for the uncertainty of the modelled elevations. The maximum value of the GIA fingerprint elevation range (blue square) corresponds to the maximum value (i.e., 7.1 m at 117 ka, MIS 5e) of the relative sea level curve generated for this study (without uplift), see Section 3.2.6 and the blue curve in Figure 4.

4.3. Observed reef facies

The modern leeward coast is dominated by a broad fringing reef, with several barrier islands protruding to the south, past Eagle Beach (Fig. 1). CRT 1 on the northwestern leeward part of the island depicts a calm, sandy back reef with semi-massive to massive solitary corals (e.g., *Diploria* spp. and *Orbicella* spp., Figs. 7A; S2-A-B-G-H). However, it is difficult to describe facies transitions within CRT 1 on the leeward coast as no exposed cross-sections (i.e., *bocas*) are present. Instead, reflecting on both the modern near-coast bathymetry and its broad, flat morphology, CRT 1 is interpreted to represent a prolonged phase of reef flat-to-lagoonal transition. The top unit of CRT 1 is closed-out by a ubiquitous layer of bioclastic infill debris, including sub-rounded to rounded branching coral clasts (i.e., *A. cervicornis,* Fig. S2-A-C-D-E-F), bivalve and *Strombus strombus* shells (Figs. 7A; S2-C-D).

Along the windward coast, the many *bocas* incising CRT 1, associated with MIS 5e, provide natural cross-sections where the reef terrace stratigraphy can be observed. In general, there are two dominant MIS 5e reef facies on this side of the island, sometimes in contact with the volcanic rock basement (i.e., Boca Windward 4, Figs. 7B; S1-B-C; S3). Of the two reef facies, the first corresponds to massive corals growing directly on the volcanic rocks (Fig. S3-C-D). It is overlain by a second facies, including *Acropora* spp.*,* bivalve shell rubble and reworked corals (Figs. 7B; S3). We interpret the lower unit as a calm-water back reef, culminating with the encrustation of *Diploria* spp. on the volcanic basement near the inner margin of CRT 1 (e.g., in Boca Windward 4). The second unit represents the MIS 5e sea level regression as inner reef flat (or shallow lagoon) transitioned into abandonment and deposition of bioclastic debris. A reef crest further seaward was probably associated with these units but has now been eroded by the sea.

The southern coast, stretching northwestwards from Seroe Colorado, has unique and well-preserved sections of all three CRTs, especially at Rincon Beach and Bachelor's Beach (Figs. S4; S5). At Rincon beach, *A. palmata* measuring several meters in diameter dominates the main unit of CRT 1, which is then overlain by an isolated *Orbicella* spp. and *Diploria* spp. unit (Fig. S4-A-B). This same succession is present at Bachelor's Beach and, while no cliff face is present, a linear topographic high stretch extends along the top of the *A. palmata* dominated facies (Fig. S4-C-D). Landward of this, a small linear depression occurs, with small, isolated *D. strigosa* exposed and associated with a fine rubble layer, including mollusk shells (Fig. 7C). These sections are characterized by a well-developed fore reef-crest-lagoon transition and indicative of a long-lasting stable relative sea-level.

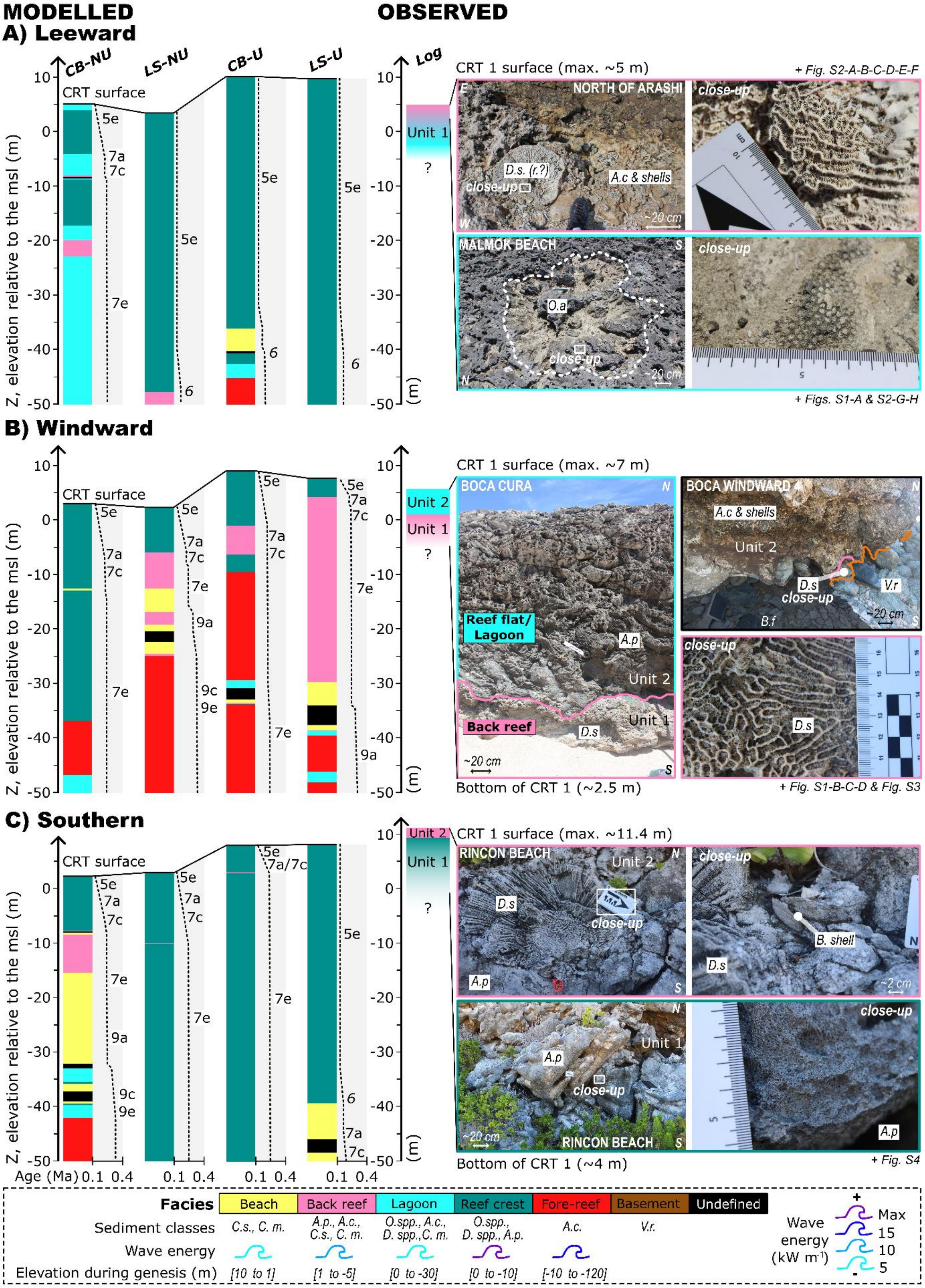

Figure 7. Comparison of modelled and observed facies for the **A)** leeward, **B)** windward, **C)** southern domains. The various parameters associated with the wells are shown in Table 6. The acronyms are defined as follows: D.s.: *Diploria strigosa*; O.a.: *Orbicella annularis*; A.p.: *Acropora palmata*. A.c.: *Acropora cervicornis*; s.: shell; V.r.: Volcanic rock; C.s.:

Carbonate sand; C.m.; Carbonate mud; B.f.: Boca floor. The elevations for the observed sites are from the dGNSS transects, have an uncertainty of ±0.1 m and are relative to the mean sea level (msl). For a more complete overview of the facies modelled, please refer to Supplementary Information S2.

4.4. Modelled reef facies

Except for the CB-NU scenario, the MIS 5e unit modelled in the leeward wells is composed exclusively of a reef crest facies (decameter thick, Fig. 7A). For the CB-NU scenario, a lagoon about 2 m thick overlies the reef crest facies (Fig. 7A). The MIS 5e unit is overlying MIS 7a reefs for the CB-NU scenario and on MIS 6 reefs for the other scenarios (Fig. 7A). No back reef facies are modelled, contrary to what we observed in the field (Figs. 7A; S2-A-B-C-D-E-F). However, the lagoon modelled in the CB-NU scenario is in line with our observations (Figs. 7A; S2-G-H). Contrasting to what we observe in the field, no volcanic rocks outcrop in our model outputs. This discrepancy likely arises from the greater thickness of the modelled reef units compared to the thin coral veneers observed in the field, as well as the absence of horizontal erosion processes within DionisosFlow® (see Discussion).

The MIS 5e unit modelled for the windward domain is dominated by a reef crest facies (about 5 m thick for all scenarios; Fig. 7B). This unit is overlying a reef crest facies for the CB-NU scenario and a back reef facies for the other scenarios, both associated with MIS 7a (Fig. 7B). The facies modelled in the selected wells are therefore at odds with our field observations. However, possibly half of what is modelled is no longer visible today, having been completely eroded. As a result, it is no longer possible to observe the fore reef and reef crest associated with MIS 5e (see Supplementary Information S2). Also, no volcanic rocks outcrop inside the model outputs.

Unit MIS 5e in the southern domain is also dominated by a reef crest facies (a few meters to ten meters thick; Fig. 7C). This is in complete agreement with our field observations (Figs. 7C; S4). The MIS 5e unit covers a reef crest facies associated with MIS 7a, with the exception of the LS-U scenario, which shows a reef crest associated with MIS 6 overlaying a MIS 7a beach (Fig. 7C).

5. Discussion

Field observations, topographic data and model outputs show significant morpho-stratigraphic differences between the fossil coral reefs of the leeward, windward and southern coasts of Aruba. After pointing out the limitations of stratigraphic forward models, we examine the roles of local vertical movement, basement slope, hydrodynamics and ecology in forcing these morphological differences.

5.1. Model limitations

As previously outlined by Boyden et al. (2023), assumptions and simplifications needed to model complex physical systems within DionisosFlow® should be considered when assessing model outputs. For example, sediment transport between grid cells is computed using a diffusion equation, and, while this method works well for large, basin-scale models, it may struggle to capture the more nuanced hydrodynamics of shallow reef environments (Barrett and Webster, 2017). Therefore, to partially mitigate this issue, the smallest possible model grid resolution is used (50 x 50 m, Table 1). Moreover, there are inherent uncertainties in identifying the key processes and environmental variables that most strongly control reef evolution, especially given that no simulation can account for all of them or fully capture the complexity of their interactions (e.g., Montaggioni et al., 2015).

Another important point is that the use of geological proxies to investigate intra-stadial sea-level fluctuations relies on their preservation (e.g., Montaggioni et al., 2015; Malatesta et al., 2022; Boyden et al., 2023). Although erosion processes are spatio-temporally variable (e.g., Chauveau et al., 2021), in our model, erosion is simplified to a constant rate of 100 m Ma^{-1} across the domain. Furthermore, as previously mentioned, DionisosFlow® does not include any wave-related erosion component (i.e., allowing horizontal erosion of emerged geological units). This contrasts with the REEF code (i.e., a coral reef evolution numerical model, Husson et al., 2018; Pastier et al., 2019), which includes a vertical sea-bed erosion and a horizontal cliff erosion component (Anderson et al., 1999).

Uncertainties in Quaternary sea-level variations are high (e.g., Caputo, 2007) and the choice of a specific curve may greatly affect the model outcome (e.g., de Gelder et al., 2020). Using only two RSL curves as input data within DionisosFlow® (Fig. 4) represents an additional limitation. Moreover, the lack of data from core drilling, seismic surveys, high-resolution nearshore bathymetry and definition of subsurface horizons in Aruba, forced us to use two bathymetric scenarios as input for the model inputs: one assuming the bathymetry was the same 400 ka ago as it is today, and another assuming a purely linear initial slope (Section 3.2.1.; Fig. 2). Also, the lack of geochronological data for Aruba is a significant limitation, introducing considerable temporal uncertainty into our interpretation. Finally, a variable spatial-temporal rate of coral growth is not considered. As no seismic data or well logs exist for the area, we assume both constant coral growth rates as well as coral growth *versus* depth curves throughout the model runs.

All of these limitations inevitably lead to model outputs that differ from reality (Figs. 6; 7). The over-thickened, offshore-extensive modelled reefs, compared to the observed ones (Fig. 6A), indicate that wave-related erosion and subaerial retreat shaped the Aruba CRTs far more than DionisosFlow® can presently capture. Moreover, the omission of the natural spatio-temporal variability of coral growth, combined with the use of a single maximum production rate as the model input for each coral species (Fig. 3), contributes to producing model outputs that are wider and thicker than the observed reefs (Fig. 6A). This may also explain the absence of volcanic outcrops in our simulations (Fig. 7). Likewise, fine-scale hydrodynamic processes (e.g., lagoonal circulation and wave-energy gradients) exert strong control on reef facies distribution (Lowe et al., 2009). However, these processes operate at scales finer than the model’s minimum grid resolution of 50 × 50 m (Table 1). This limitation likely accounts for the discrepancies between the modelled and observed reef facies (Fig. 7). For example, the thin and spatially restricted units observed in the field, such as the few-meter-thick back-reef facies on the southern coast (Unit 2, Fig. 7C), are not reproduced in the simulations. Collectively, these discrepancies highlight the need to incorporate wave-related erosion, fine-scale hydrodynamics, and variable coral growth rates into future models to more faithfully reproduce the real coral reef system. Despite these limitations, our model outputs provide key insights into the origins of the intra-island morpho-stratigraphic differences observed in Aruba’s coral reefs.

5.2. North-to-south morphological discrepancies

Our dGNSS transects show a difference in the elevation of CRT 1 between the leeward, windward and southern coasts of the island (Fig. 5). The maximum surveyed elevation of CRT 1 is at 4.26 ±1.4 m apmsl in average (3 transects) on the leeward coast, 6.85 ±1.51 m apmsl in average for the windward coast (11 transects), while it is 10.84 ±0.66 m apmsl along the southern coast (4 transects; Pet cemetery and Bachelor s Beach sites). Also, most of the northern part of Aruba is characterized by a single terrace, while the southern coast is characterized by a staircase of three terraces (Figs.

2; 5). These discrepancies in elevation and number of terraces in the sequence led us to investigate the role of uplift in the morphogenesis of the CRT sequence of each domain. The model successfully reproduces these features, yielding a single MIS 5e terrace with a maximum elevation of 7.1 m apmsl under no-uplift scenarios, and a sequence of three, higher-elevation terraces for the scenarios with an uplift rate of 0.05 mm a^{-1} (illustrated for the southern domain in Fig. 8; see Supplementary Information S2).

One possible explanation for the north-to-south morphological difference could be differential tectonic uplift across the island of Aruba. Geodynamic land motion of the Quaternary CRT sequence of Aruba is related either to the southward shallow subduction of the Caribbean plate or to active folding or faulting (Hippolyte & Mann, 2011). Northwest-striking faults cutting the sequence may be responsible for a recent reactivation of the Neogene normal faults of the island (Fig. 1B; Beets, 1996), which would be compatible with GPS measurements showing differential motion along the south Caribbean margin (Pérez et al., 2001; Trenkamp et al., 2002) and seafloor offsets offshore Curaçao indicating recent normal fault movements (Gorney et a., 2007). This could explain the slight uplift of CRTs in the southern coast of Aruba, resulting in the present-day exposure of reefs likely formed during MIS 5e (CRT I), MIS 9c/9e (CRT II), and MIS 11c (CRT III) (Fig. 8), whereas a single MIS 5e terrace would be exposed in the northern part of the island, probably unaffected by uplift (leeward and windward coasts). Indeed, the CRT 1 elevation in the north of Aruba (both leeward and windward domains) can be explained solely by our RSL curve without the uplift component, and therefore by the effects of the GIA in the area (maximum relative sea level of 7.1 m apmsl, 117 ka ago, Fig. 4). Moreover, relatively stable tectonics favor successive reoccupation of different sea-level highstands (e.g., MIS 9a by MIS 7e or MIS 7e by MIS 5e, e.g., Pastier et al., 2019). This leads to a single emerged CRT composed of several reefal limestone units of different ages, as observed on Curaçao (an MIS 5e unit overlying an MIS 7a/7c unit, Muhs et al., 2012) and modelled by this work (Figs. 7; 8; Supplementary Information S2).

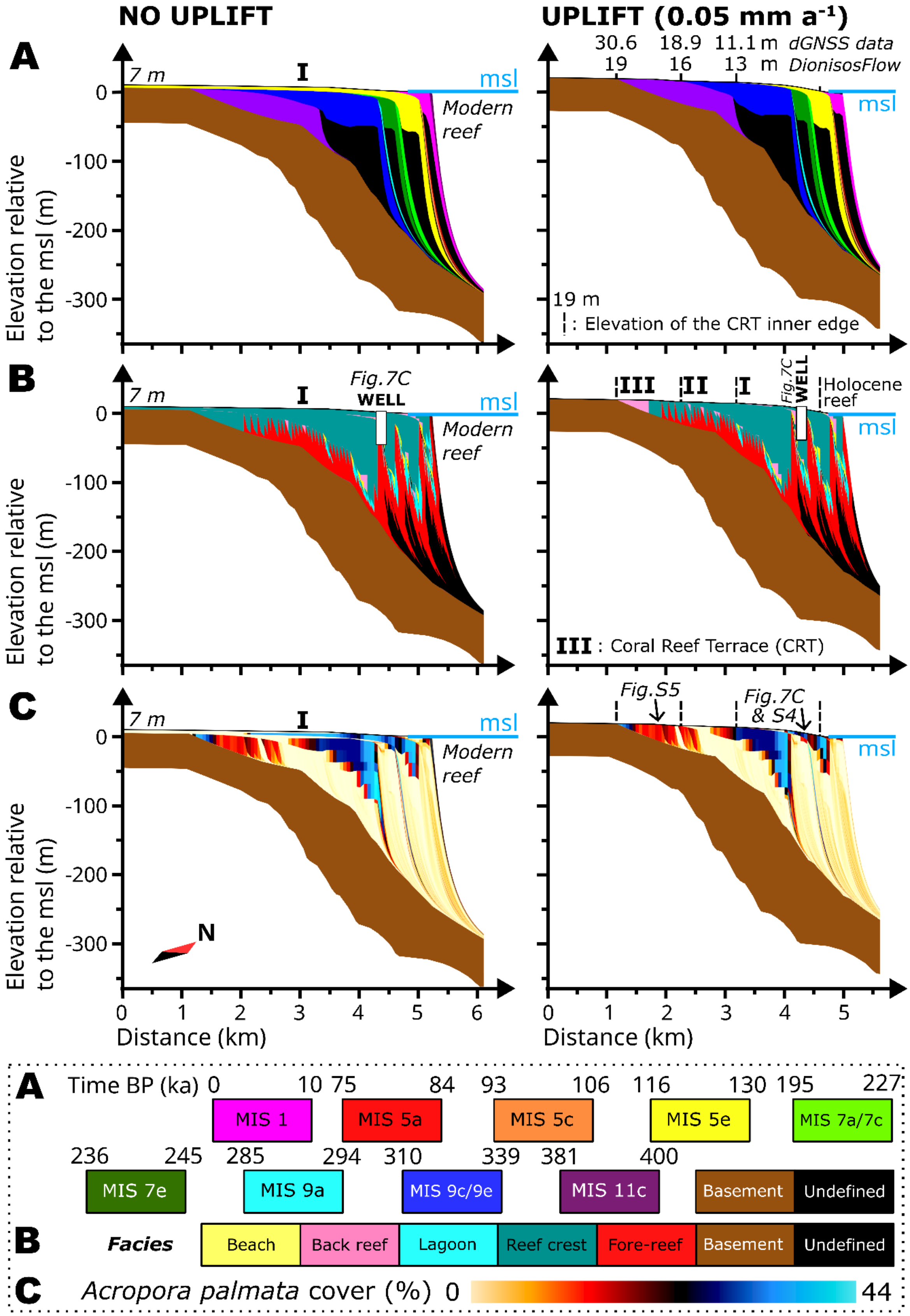
NO UPLIFT
UPLIFT (0.05 mm a^{-1})
A
B
C
30.6 18.9 11.1 m dGNSS data
19 16 13 m DionisosFlow
7 m
I
II
III
msl
Modern reef
Holocene reef
Fig.7C
WELL
Fig.S5
Fig.7C & S4
19 m
¦ : Elevation of the CRT inner edge
III : Coral Reef Terrace (CRT)
N
Elevation relative to the msl (m)
0
-100
-200
-300
Distance (km)
0
1
2
3
4
5
6
Time BP (ka) 0 10 75 84 93 106 116 130 195 227
MIS 1
MIS 5a
MIS 5c
MIS 5e
MIS 7a/7c
236 245 285 294 310 339 381 400
MIS 7e
MIS 9a
MIS 9c/9e
MIS 11c
Basement
Undefined
Facies
Beach
Back reef
Lagoon
Reef crest
Fore-reef
Basement
Undefined
Acropora palmata cover (%) 0
44

Figure 8. Comparison of model outputs for the southern domain, without and with an uplift rate of 0.05 mm a^{-1}, classified by **A)** Marine Isotope Stage (MIS), **B)** facies and **C)** *A. palmata* cover percentage. The timing of the MIS is identified on the RSL curve used in this study. The model outputs are those of the current bathymetry scenario (i.e., CB). Elevations from dGNSS transects have an uncertainty of ±0.1 m, while those from DionisosFlow® have an uncertainty of ±0.5 m. The basement facies layer does not have a regular thickness (i.e., the 50 m defined as model input) because the CB (i.e., Current-Bathymetry) scenario has an irregular bathymetry and Figure 8 is a 2D section of a 3D model. For a more detailed view of the 3D model please refer to Supplementary Information S2.

5.3. Initial bathymetry

Models constrained by present-day bathymetry (Current-Bathymetry, CB, scenarios) align more closely with observed terrace morphologies than those assuming a linear volcanic basement slope (Linear Slope, LS, scenarios). Given the improbability of initial linear topography for terraced landscape, scenarios incorporating current bathymetry more accurately represent bedrock complexity and thus more faithfully reproduce present-day sequence morphologies (Figs. 7; 8; Supplementary Information S2).

The slope of the basement upon which coral reefs can grow plays a central role in the available accommodation space, and therefore in their offshore extension (e.g., Camoin & Webster, 2015; Pastier et al., 2019). Our leeward domain has a gentle basement slope, while the windward domain is much steeper, 3.1% vs 19% respectively (Table 1). As a result, our model simulates a narrower reef on the windward coast compared to the leeward (Fig. 6A; Supplementary Information S2). The steeper the basement slope, the narrower the reefs and the greater the erosion efficiency, leading to a negative erosional feedback loop (Chauveau et al., 2024b). This phenomenon is further exacerbated by the difference in wave energy between the leeward and windward domains (Table 3). This results in rapid erosion of the emerged reefs on the north windward coast and could also explains the absence of fossil reefs older than MIS 5e, which are eroded with each subsequent sea-level highstand. Erosional processes, coupled with a likely negligible uplift rate in the northern part of the island (i.e., leeward and windward coasts), led to the growth of MIS 5e corals directly on the volcanic bedrock. However, we cannot model this phenomenon as the hydrodynamic component in DionisosFlow® has no erosive effect but only influences depositional factors.

5.4. Ecology: the influence of *A. palmata*

The presence of *A. palmata* seems to play a key role in the spatial distribution of reef facies in the fossil record. In fact, the maximum percentage of *A. palmata* constitutes ~34% for the leeward domain, compared with ~44% and ~50% for the southern and windward domains (CB-U scenario), respectively. The higher the wave energy, the more favorable the environment for *A. palmata* growth as well as further recruitment (Table 2; Lirman, 2000). This, in combination with fast growth rates, allows for *A. palmata* to dominate and outcompete other more massive or delicate growth forms under ideal conditions (e.g., *Orbicella* spp. and *A. cervicornis*, Porto-Hannes et al., 2015. Figs. 7B-C; S4), leading to a dominance of reef crest and back reef facies on the windward and southern coasts (Figs. 7B, 7C; S3; S4).

Finally, paleo sea-level indicators derived independently from either leeward, windward and southern reef morphologies would stand in contrast to those derived by the other. Therefore, while accommodation space is the main driver in interstadial reef growth cycles (e.g., Camoin and Webster 2015), CRT derived paleo sea-level index point accuracy is directly contingent upon the inclusion of localized dynamics governing reef growth in the past.

6. Conclusion

The study of past sea-level variations using fossil coastlines is an essential tool to understand modern local and global changes in sea level. Coral reefs are among the most accurate sea-level index points to gauge such changes. Here, we show that hydrodynamic and ecological local characteristics may be the source of morphological asymmetries at very small spatial scales. In this work, we focused on the island of Aruba, which is characterized by a strong asymmetry of the coral reef sequence due to prevailing winds and associated wave energy. We use stratigraphic forward modelling, supported by a dataset of dGNSS transects, SfM/MVS surveys, and ecological descriptions, to quantify and find an explanation for such morphological discrepancies. Three factors emerge as potential sources for the differences observed in the coral reef fossil record: (1) local vertical movements, (2) basement slope and (3) environmental factors favoring particular reef frameworks. Our results show that the difference in elevation between the northern and southern terraces of Aruba (6.85 ±1.51 m vs 10.84 ±0.66 m, respectively) could conceivably result from local vertical movements. Finally, our modelling outputs show that a steep basement slope associated with a high percentage of *A. palmata*, linked to strong hydrodynamic conditions, will lead to the genesis of narrow reefs dominated by reef crest facies (i.e., windward and southern coasts). On the contrary, a gentle basement slope with calm hydrodynamic conditions will favor the growth of wide reefs dominated by back reefs and lagoons colonized predominately by massive corals (i.e., leeward coast). These two contrasting coral reef terrace morphologies, within close proximity and deposited under the same MIS 5e relative sea-level highstand, highlight the precarious nature of deriving paleo sea-level and tectonic histories from single coral reef terrace records.

Supplementary Information

The supplementary information includes files containing figures with the field observations (Supplementary Information 1, figures S1-S5) and with the model outputs (Supplementary Information 1, figures S6-S29).

Data availability

dGNSS transect data and forward stratigraphic model input files (workflows and data) are available online (https://doi.org/10.5281/zenodo.14899366) from Chauveau et al., (2025b). The 3D stratigraphic forward model DionisosFlow® (*IFP Energies nouvelles* / Beicip-Franlab) is available upon request at: https://www.beicip.com/contact/.

Acknowledgements

This paper is a result of the WARMCOASTS project, funded by the European Research Council (ERC) under the European Union’s Horizon 2020 research and innovation programme (grant agreement n. 802414 to Alessio Rovere). This paper reflects only the authors view and that the EU is not responsible for any use that may be made of the information it contains. This work is part of the "Frozen in time" project, funded by the Deutsche Forschungsgemeinschaft (DFG, German Research Foundation) – Project number 468589501 (Patrick Boyden & Sonia Bejarano) – SPP 2299/Project number 441832482. This work is also part of the PLOMA project (led by Denovan Chauveau) which is supported by ISblue project, Interdisciplinary graduate school for the blue planet (ANR-17-EURE-0015) and co-funded by a grant from the French government under the program "Investissements d'Avenir" embedded in France 2030. This work has been partially funded by the Research Agreement stipulated between the University of Bari Aldo Moro and the Agenzia Regionale Strategica per lo Sviluppo Ecosostenibile del Territorio (ASSET, Italy) (Scientific Coordinator Giovanni Scicchitano). We would like to thank Beicip-Franlab for providing an academic license to OpenFlow Suite and DionisosFlow® v2024.1. We also thank the staff members of the Aruba National Park Foundation (FPNA): Natasha Silva and Sietske van der Wal, for their availability and warm welcome. We would like to thank Sebastiano Orlando Facchin for his contribution to the mapping work, Blake Dyer and Jacqueline Austermann for sharing the GIA predictions for Aruba. In this work, we use the global wave hindcast data from the Centre for Australian Weather and Climate Research (CAWCR), a partnership between the Bureau of Meteorology and CSIRO. Hindcast modelling undertaken as part of the PACCSAP (Pacific-Australia Climate Change Science and Adaptation Planning) Project 4.3 "High resolution wind-wave climate and projections of change in the Pacific region for coastal hazard assessments" in 2012, and extended with support from COSPPAC (Climate and Oceans Support Program in the Pacific). This project was funded by DCCEE and AusAID and undertaken jointly by CSIRO and the BoM. Model run on the Bureau of Meteorology SOLAR facility and NGAMAI facility. TanDEM-X digital elevation data are under copyright by the German Aerospace Center (all rights reserved) and are used herein with permission within Project DEM GEOL1210 (Alessio Rovere and Maureen E. Raymo). The authors acknowledge PALSEA, a working group of the International Union for Quaternary Sciences (INQUA) and Past Global Changes (PAGES), which in turn received support from the Swiss Academy of Sciences and the Chinese Academy of Sciences. Finally, we would like to thank the editor, Jaap Nienhuis, and the two anonymous reviewers for their constructive comments and reviews, which helped improve the article.

Authors Credit

DC carried out the modelling and wrote the article with inputs from PB and AR. DC, PB, AR, GS and GS took part field surveys. PB provided dGNSS data

and photogrammetry data (DEM and Orthomosaic). FD and PB helped to build the models with DionisosFlow®. SD helped with the relative sea level curve adopted in the work. EM helped in organizing fieldwork and contributed local knowledge. SB and CC brought valuable ideas to the project on, respectively, modern and fossil coral reef ecology. All co-authors reviewed the article, suggested implementations to the text and agree with its contents.

Conflict of Interest Disclosure

The authors declare that they have no known competing financial interests, personal relationships, or conflicts of interest that could have appeared to influence the work reported in this article.

References

1. **Alexander**, C. S. (**1961**). The marine terraces of Aruba, Bonaire, and Curaçao, Netherlands Antilles. Annals of the Association of American Geographers, 51(1), 102-123. https://doi.org/10.1111/j.1467-8306.1961.tb00370.x
2. **Anderson**, R.S., Densmore, A.L., Ellis, M.A., (**1999**). The generation and degradation of marine terraces. Basin Res. 11 (1), 7–20. https://doi.org/10.1046/j.1365-2117.1999.00085.x.
3. **Andres**, M., Bassant, Ph. and Harris, M. (**2008**) Conditioned forward stratigraphic modeling in large carbonate fields: a Dionisos model of Karachaganak. Search and Discovery Article #40352.
4. **Austermann**, J., Mitrovica, J. X., Huybers, P., & Rovere, A. (**2017**). Detection of a dynamic topography signal in last interglacial sea-level records. *Science Advances*, *3*(7), e1700457. DOI: 10.1126/sciadv.1700457
5. **Avé Lallemant**, H. G. (**1997**). Transpression, displacement partitioning, and exhumation in the eastern Caribbean/South American plate boundary zone. *Tectonics*, *16*(2), 272-289. https://doi.org/10.1029/96TC03725
6. **Barnett**, R. L., Austermann, J., Dyer, B., Telfer, M. W., Barlow, N. L., Boulton, S. J., ... & Creel, R. C. (**2023**). Constraining the contribution of the Antarctic Ice Sheet to Last Interglacial sea level. *Science Advances*, *9*(27), eadf0198. DOI: 10.1126/sciadv.adf0198

7. **Barrett**, S. J., & **Webster**, J. M. (**2012**). Holocene evolution of the Great Barrier Reef: Insights from 3D numerical modelling. *Sedimentary Geology*, *265*, 56-71. https://doi.org/10.1016/j.sedgeo.2012.03.015
8. **Bassant**, Ph. and **Harris**, M. (**2008**) Analyzing reservoir architecture of isolated carbonate platforms. Search and Discovery Article #40295.
9. **Beardsley**, A. G., & **Avé Lallemant**, H. G. (**2007**). Oblique collision and accretion of the Netherlands Leeward Antilles to South America. *Tectonics*, *26*(2). https://doi.org/10.1029/2006TC002028
10. **Beets**, D., (**1996**). Geological Map of Aruba. Scale 1:50 000. Foundation for Scientific Research in the Caribbean region, and geological Survey of the Netherlands (RGD) (Eds)
11. **Boyden**, P., Stocchi, P., and Rovere, A. "Refining patterns of melt with forward stratigraphic models of stable Pleistocene coastlines." Earth Surface Dynamics 11.5 (**2023**): 917-931. https://doi.org/10.5194/esurf-11-917-2023, 2023
12. **Burgess**, P.M. and Wright, V.P. (**2003**) Numerical forward modeling of carbonate platform dynamics: an evaluation of complexity and completeness in carbonate strata. J. Sed. Res., 73, 637–652.
13. **Burgess**, P.M., Lammers, H., van Oosterhout, C. and Granjeon, D. (**2006**) Multivariate sequence stratigraphy: tackling complexity and uncertainty with stratigraphic forward modelling, multiple scenarios and conditional frequency maps. AAPG Bull., 90, 1883–1901.
14. **Burgess**, P. M., & **Pollitt**, D. A. (**2012**). The origins of shallow-water carbonate lithofacies thickness distributions: one-dimensional forward modelling of relative sea-level and production rate control. *Sedimentology*, *59*(1), 57-80. https://doi.org/10.1111/j.1365-3091.2011.01303.x
15. **Camoin**, G. F., & **Webster**, J. M. (**2015**). Coral reef response to Quaternary sea-level and environmental changes: State of the science. Sedimentology, 62(2), 401-428. https://doi.org/10.1111/sed.12184
16. **Chappell**, J. (**1974**). Geology of coral terraces, Huon Peninsula, New Guinea: a study of Quaternary tectonic movements and sea-level changes. *Geological Society of America Bulletin*, *85*(4), 553-570. https://pubs.geoscienceworld.org/gsa/gsabulletin/article/85/4/553/201595/Geology-of-Coral-Terraces-Huon-Peninsula-New
17. **Chauveau**, D., Authemayou, C., Pedoja, K., Molliex, S., Husson, L., Scholz, D., ... & Aster Team. (**2021**). On the generation and degradation of emerged coral reef terrace sequences: First cosmogenic 36Cl analysis at Cape Laundi, Sumba Island (Indonesia). Quaternary Science Reviews, 269, 107144. https://doi.org/10.1016/j.quascirev.2021.107144
18. **Chauveau**, D., Pastier, A. M., de Gelder, G., Husson, L., Authemayou, C., Pedoja, K., & Cahyarini, S. Y. (**2024a**). Unravelling the morphogenesis of coastal terraces at Cape Laundi (Sumba Island, Indonesia): Insights from numerical models. Earth Surface Processes and Landforms, 49(2), 549-566. https://doi.org/10.1002/esp.5720
19. **Chauveau**, D., Georgiou, N., Cerrone, C., Dean, S., & Rovere, A. (**2024b**). Sea-level oscillations within the Last Interglacial: insights from coral reef stratigraphic forward modelling. Quaternary Science Reviews, 336, 108759. https://doi.org/10.1016/j.quascirev.2024.108759
20. **Chauveau**, D., Pedoja, K., Authemayou, C., Husson, L., de Gelder, G., Aribowo, S., ... & Cahyarini, S. Y. (**2025a**). Morphogenesis of the Holocene coastal landforms on Sumba Island, Indonesia. *Journal of Asian Earth Sciences: X*, *14*, 100208. https://doi.org/10.1016/j.jaesx.2025.100208

21. **Chauveau**, D., Boyden, P., Desfromont, F., Scardino, G., Scicchitano, G., Mijts, E., Bejarano, S., Dean, S., Cerrone, C., & Rovere, A. (**2025b**). Dataset from Chauveau et al. "Unravelling the spatial variability of fossil coral reef morphology on Aruba and the implications for paleo sea level estimates". (Version 1) [Dataset]. Zenodo. https://doi.org/10.5281/zenodo.14899366

22. **Chutcharavan**, P. M., & **Dutton**, A. (**2021**). A global compilation of U-series-dated fossil coral sea-level indicators for the Last Interglacial period (Marine Isotope Stage 5e). Earth System Science Data, 13(7), 3155-3178. https://doi.org/10.5194/essd-13-3155-2021

23. **Claps**, M., Zempolich, W.G., Casaglia, F. and Ronchi, P. (**2009**) Sedimentology and Stratigraphy of the Kashagan Buildup, Carboniferous, Pricaspian Basin, Kasakhstan. Abstract, Search and Discovery Article #90090, AAPG Meeting, Denver, CO.

24. **Davis**, K.L., Colefax, A.P., Tucker, J.P. et al. Global coral reef ecosystems exhibit declining calcification and increasing primary productivity. Commun Earth Environ 2, 105 (**2021**). https://doi.org/10.1038/s43247-021-00168-w

25. **DeConto**, R. M., Pollard, D., Alley, R. B., Velicogna, I., Gasson, E., Gomez, N., ... & Dutton, A. (**2021**). The Paris Climate Agreement and future sea-level rise from Antarctica. Nature, 593(7857), 83-89. https://doi.org/10.1038/s41586-021-03427-0

26. **de Buisonjé**, P. H. (**1974**). Neogene and quaternary geology of Aruba, Curaçao and Bonaire. *PhD thesis, Universiteit van Amsterdam*.

27. **de Gelder**, G., Jara-Munoz, J., Melnick, D., Fernández-Blanco, D., Rouby, H., Pedoja, K., ... & Lacassin, R. (**2020**). How do sea-level curves influence modeled marine terrace sequences?. Quaternary Science Reviews, 229, 106132. https://doi.org/10.1016/j.quascirev.2019.106132

28. **de Gelder**, G., Husson, L., Pastier, A. M., Fernández-Blanco, D., Pico, T., Chauveau, D., ... & Pedoja, K. (**2022**). High interstadial sea levels over the past 420ka from the Huon Peninsula, Papua New Guinea. Communications Earth & Environment, 3(1), 256. https://doi.org/10.1038/s43247-022-00583-7

29. **de Gelder**, G., Solihuddin, T., Utami, D. A., Hendrizan, M., Rachmayani, R., Chauveau, D., ... & Cahyarini, S. Y. (**2023**). Geodynamic control on Pleistocene coral reef development: Insights from northwest Sumba Island (Indonesia). Earth Surface Processes and Landforms, 48(13), 2536-2553. https://doi.org/10.1002/esp.5643

30. **Dewar**, R. E., & Richard, A. F. (**2007**). Evolution in the hypervariable environment of Madagascar. *Proceedings of the National Academy of Sciences*, *104*(34), 13723-13727. https://doi.org/10.1073/pnas.0704346104

31. **Dullo**, W. C. (**2005**). Coral growth and reef growth: a brief review. *Facies*, *51*(1), 33-48. https://doi.org/10.1007/s10347-005-0060-y

32. **Dumitru**, O. A., Dyer, B., Austermann, J., Sandstrom, M. R., Goldstein, S. L., D'Andrea, W. J., ... & Raymo, M. E. (**2023**). Last interglacial global mean sea level from high-precision U-series ages of Bahamian fossil coral reefs. Quaternary Science Reviews, 318, 108287. https://doi.org/10.1016/j.quascirev.2023.108287

33. **Dutch Caribbean Biodiversity Database** [WWW Document], 2019. URL632 https://www.dcbd.nl/resource/2319 (accessed 7.22.24).

34. **Dutton**, A., Carlson, A. E., Long, A. J., Milne, G. A., Clark, P. U., DeConto, R., ... & Raymo, M. E. (**2015**). Sea-level rise due to polar ice-sheet mass loss during

past warm periods. *science*, *349*(6244), aaa4019. DOI: 10.1126/science.aaa4019

35. **Durrant**, Thomas; Hemer, Mark; Trenham, Claire; & Greenslade, Diana (**2013**): CAWCR Wave Hindcast 1979-2010. v10. CSIRO. Service Collection. http://hdl.handle.net/102.100.100/13165?index=1
36. **Dyer**, B., Austermann, J., D'Andrea, W. J., Creel, R. C., Sandstrom, M. R., Cashman, M., ... & Raymo, M. E. (**2021**). Sea-level trends across The Bahamas constrain peak last interglacial ice melt. *Proceedings of the National Academy of Sciences*, *118*(33), e2026839118. https://doi.org/10.1073/pnas.2026839118
37. **Fouke**, B. W., Beets, C. J., Meyers, W. J., Hanson, G. N., & Melillo, A. J. (**1996**). 87 Sr/86 Sr Chronostratigraphy and dolomitization history of the Seroe Domi Formation, Curaçao (Netherlands Antilles). *Facies*, *35*, 293-320. https://doi.org/10.1007/BF02536966
38. B. **Fox-Kemper**, H.T. Hewitt, C. Xiao, G. Aðalgeirsdóttir, S.S. Drijfhout, T. L. Edwards, N.R. Golledge, M. Hemer, R.E. Kopp, G. Krinner, A. Mix, D. Notz, S. Nowicki, I.S. Nurhati, L. Ruiz, J.-B. Sallée, A.B.A. Slangen, Y. Yu, Ocean, cryosphere and sea level change, in Climate Change **2021**: The Physical Science Basis. Contribution of Working Group I to the Sixth Assessment Report of the Intergovernmental Panel on Climate Change, V. Masson-Delmotte, P. Zhai, A. Pirani, S.L. Connors, C. Péan, S. Berger, N. Caud, Y. Chen, L. Goldfarb, M.I. omis, M. Huang, K. Leitzell, E. Lonnoy, J.B.R. Matthews, T.K. Maycock, T. Waterfield, O. Yelekçi, R. Yu, B. Zhou, Eds.(Cambridge Univ. Press, 2021), pp. 1211–1362.
39. **Gardner**, T. A., Côté, I. M., Gill, J. A., Grant, A., & Watkinson, A. R. (**2005**). Hurricanes and Caribbean coral reefs: impacts, recovery patterns, and role in long-term decline. *Ecology*, *86*(1), 174-184. https://doi.org/10.1890/04-0141
40. **Granjeon**, D., & **Joseph**, P. (**1999**). Concepts and applications of a 3-D multiple lithology, diffusive model in stratigraphic modeling.
41. **Granjeon**, D. (**1997**) Modélisation stratigraphique déterministe: conception et applications d'un modèle diffusif 3D multilithologique. Thèse Doct. University of Rennes 1, France, 175 pp.
42. **Granjeon**, D., Masson, R. and Wolf, S. (**2005**) Modélisation stratigraphique 3D en zones tectoniques complexes. Rapport IFP 58598.
43. **Gischler**, E., Hudson, J. H., Humblet, M., Braga, J. C., Schmitt, D., Isaack, A., ... & Camoin, G. F. (**2019**). Holocene and Pleistocene fringing reef growth and the role of accommodation space and exposure to waves and currents (Bora Bora, Society Islands, French Polynesia). *Sedimentology*, *66*(1), 305-328. https://doi.org/10.1111/sed.12533
44. **Gorney**, D., Escalona, A., Mann, P., Magnani, M. B., & BOLIVAR Study Group. (**2007**). Chronology of Cenozoic tectonic events in western Venezuela and the Leeward Antilles based on integration of offshore seismic reflection data and on-land geology. *AAPG bulletin*, *91*(5), 653-684.
45. **Herweijer**, J. P., & Focke, J. W. (**1978**). On the Pleistocene sea level history of the Netherlands Antilles. *Geol. Mijnbouw*.
46. **Hibbert**, F. D., Rohling, E. J., Dutton, A., Williams, F. H., Chutcharavan, P. M., Zhao, C., & Tamisiea, M. E. (**2016**). Coral indicators of past sea-level change: A global repository of U-series dated benchmarks. *Quaternary Science Reviews*, *145*, 1-56. https://doi.org/10.1016/j.quascirev.2016.04.019

47. **Hippolyte**, J. C., & **Mann**, P. (**2011**). Neogene–Quaternary tectonic evolution of the Leeward Antilles islands (Aruba, Bonaire, Curaçao) from fault kinematic analysis. *Marine and Petroleum Geology*, *28*(1), 259-277. https://doi.org/10.1016/j.marpetgeo.2009.06.010
48. **Holthuijsen**, L. H.: Waves in Oceanic and Coastal Waters (**2007**). Cambridge University Press, Cambridge, https://doi.org/10.1017/CBO9780511618536,.
49. **Holthuijsen**, L. H. (**2010**). *Waves in oceanic and coastal waters*. Cambridge university press. https://doi.org/10.1017/CBO9780511618536
50. **Horton**, B. P., Khan, N. S., Cahill, N., Lee, J. S., Shaw, T. A., Garner, A. J., ... & Rahmstorf, S. (**2020**). Estimating global mean sea-level rise and its uncertainties by 2100 and 2300 from an expert survey. NPJ climate and atmospheric science, 3(1), 18. https://doi.org/10.1038/s41612-020-0121-5
51. **Husson**, L., Pastier, A. M., Pedoja, K., Elliot, M., Paillard, D., Authemayou, C., ... & Cahyarini, S. Y. (**2018**). Reef carbonate productivity during quaternary sea level oscillations. Geochemistry, Geophysics, Geosystems, 19(4), 1148-1164. https://doi.org/10.1002/2017GC007335
52. **Kennedy**, D. M., T. H. Marsters, J. L. D. Woods and C. D. Woodroffe (**2012**). "Shore platform development on an uplifting limestone island over multiple sea-level cycles, Niue, South Pacific." Geomorphology 141: 170-182. https://doi.org/10.1016/j.geomorph.2011.12.041
53. **Koelling**, M., Webster, J.M., Camoin, G., Iryu, Y., Bard, E. & Seard, C. (**2009**) SEALEX-internal reef chronology and virtual drill logs from a spreadsheet-based reef growth model. Global and Planetary Change, 66(1–2), 149–159. https://doi.org/10.1016/j.gloplacha.2008.07.011
54. **Lajoie**, K. R. (**1986**). Coastal Tectonics. Active tectonic. N. A. Press. Washington D,C, National Academic Press**:** 95-124.
55. **Lee**, E. Y., Kominz, M., Reuning, L., Gallagher, S. J., Takayanagi, H., Ishiwa, T., Knierzinger, W., and Wagreich, M. (**2021**). Quantitative compaction trends of Miocene to Holocene carbonates off the west coast of Australia, Aust. J. Earth Sci., 68, 1149–1161, https://doi.org/10.1080/08120099.2021.1915867
56. **Lirman**, D. (**2000**). Fragmentation in the branching coral Acropora palmata (Lamarck): growth, survivorship, and reproduction of colonies and fragments. *Journal of Experimental Marine Biology and Ecology*, *251*(1), 41-57. https://doi.org/10.1016/S0022-0981(00)00205-7
57. **Lorscheid**, T., Felis, T., Stocchi, P., Obert, J. C., Scholz, D., & Rovere, A. (**2017**). Tides in the Last Interglacial: insights from notch geometry and palaeo tidal models in Bonaire, Netherland Antilles. *Scientific Reports*, *7*(1), 16241. https://doi.org/10.1038/s41598-017-16285-6
58. **Lowe**, R. J., Falter, J. L., Monismith, S. G., & Atkinson, M. J. (**2009**). Wave-driven circulation of a coastal reef–lagoon system. *Journal of Physical Oceanography*, *39*(4), 873-893. https://doi.org/10.1175/2008JPO3958.1
59. **Malatesta**, L. C., Finnegan, N. J., Huppert, K. L., & Carreño, E. I. (**2022**). The influence of rock uplift rate on the formation and preservation of individual marine terraces during multiple sea-level stands. *Geology*, *50*(1), 101-105. https://doi.org/10.1130/G49245.1
60. **Meyer**, D., Bries, J., Greenstein, B., & Debrot, A. (**2003**). Preservation of in situ reef framework in regions of low hurricane frequency: Pleistocene of Curaçao and Bonaire, southern Caribbean. *Lethaia*, *36*(3), 273-285. https://doi.org/10.1080/00241160310004675

61. **Mitrovica**, J. X., & **Milne**, G. A. (**2003**). On post-glacial sea level: I. General theory. *Geophysical Journal International*, *154*(2), 253-267. https://doi.org/10.1046/j.1365-246X.2003.01942.x

62. **Montaggioni**, L. F., & **Braithwaite**, C. J. (**2009**). *Quaternary coral reef systems: history, development processes and controlling factors*. Elsevier.

63. **Montaggioni**, L. F., Borgomano, J., Fournier, F., & Granjeon, D. (**2015**). Quaternary atoll development: New insights from the two-dimensional stratigraphic forward modelling of Mururoa Island (Central Pacific Ocean). Sedimentology, 62(2), 466-500. https://doi.org/10.1111/sed.12175

64. **Muhs**, D. R., Pandolfi, J. M., Simmons, K. R., & Schumann, R. R. (**2012**). Sea-level history of past interglacial periods from uranium-series dating of corals, Curaçao, Leeward Antilles. doi:10.1016/j.yqres.2012.05.008

65. **Murray-Wallace**, C. and C. **Woodroffe** (**2014**). Quaternary sea level : a global perspective. Cambridge, Cambridge University Press.

66. **Obert**, J. C., Scholz, D., Felis, T., Brocas, W. M., Jochum, K. P., & Andreae, M. O. (**2016**). 230Th/U dating of Last Interglacial brain corals from Bonaire (southern Caribbean) using bulk and theca wall material. *Geochimica et Cosmochimica Acta*, *178*, 20-40. https://doi.org/10.1016/j.gca.2016.01.011

67. **Pandolfi**, J. M., & **Jackson**, J. B. (**2001**). Community structure of Pleistocene coral reefs of Curaçao, Netherlands Antilles. *Ecological monographs*, *71*(1), 49-67. https://doi.org/10.1890/0012-9615(2001)071[0049:CSOPCR]2.0.CO;2

68. **Pastier**, A. M., Husson, L., Pedoja, K., Bézos, A., Authemayou, C., Arias-Ruiz, C., & Cahyarini, S. Y. (**2019**). Genesis and architecture of sequences of Quaternary coral reef terraces: Insights from numerical models. Geochemistry, Geophysics, Geosystems, 20(8), 4248-4272. https://doi.org/10.1029/2019GC008239

69. **Pavlis**, N. K., Holmes, S. A., Kenyon, S. C., & Factor, J. K. (**2012**). The development and evaluation of the Earth Gravitational Model 2008 (EGM2008). *Journal of geophysical research: solid earth*, *117*(B4). https://doi.org/10.1029/2011JB008916

70. **Pedoja**, K., Husson, L., Regard, V., Cobbold, P. R., Ostanciaux, E., Johnson, M. E., ... & Delcaillau, B. (**2011**). Relative sea-level fall since the last interglacial stage: are coasts uplifting worldwide?. *Earth-Science Reviews*, *108*(1-2), 1-15. https://doi.org/10.1016/j.earscirev.2011.05.002

71. **Pedoja**, K., Husson, L., Bézos, A., Pastier, A. M., Imran, A. M., Arias-Ruiz, C., ... & Choblet, G. (**2018**). On the long-lasting sequences of coral reef terraces from SE Sulawesi (Indonesia): Distribution, formation, and global significance. Quaternary Science Reviews, 188, 37-57. https://doi.org/10.1016/j.quascirev.2018.03.033

72. **Pérez**, O. J., Bilham, R., Bendick, R., Velandia, J. R., Hernández, N., Moncayo, C., ... & Kozuch, M. (**2001**). Velocity field across the southern Caribbean plate boundary and estimates of Caribbean/South-American plate motion using GPS geodesy 1994–2000. *Geophysical Research Letters*, *28*(15), 2987-2990. https://doi.org/10.1029/2001GL013183

73. **Pirazzoli**, P. A., Radtke, U., Hantoro, W. S., Jouannic, C., Hoang, C. T., Causse, C., & Best, M. B. (**1991**). Quaternary raised coral-reef terraces on Sumba Island, Indonesia. Science, 252(5014), 1834-1836. DOI: 10.1126/science.252.5014.1834

74. **Porto-Hannes**, I., Zubillaga, A. L., Shearer, T. L., Bastidas, C., Salazar, C., Coffroth, M. A., & Szmant, A. M. (**2015**). Population structure of the corals Orbicella faveolata and Acropora palmata in the Mesoamerican Barrier Reef System with comparisons over Caribbean basin-wide spatial scale. *Marine Biology*, *162*, 81-98. https://doi.org/10.1007/s00227-014-2560-1

75. **Rabineau**, M., Berné, S., Aslanian, D., Olivet, J.L., Joseph, P., Guillocheau, F., Bourillet, J.F., Ledrezen, E. and Granjeon, D. (**2005**) Sedimentary sequences in the Gulf of Lion: a record of 100,000 years climatic cycles. Mar. Petrol. Geol., 22, 775–804.

76. **Railsback**, L. B., Gibbard, P. L., Head, M. J., Voarintsoa, N. R. G., & Toucanne, S. (**2015**). An optimized scheme of lettered marine isotope substages for the last 1.0 million years, and the climatostratigraphic nature of isotope stages and substages. *Quaternary Science Reviews*, *111*, 94-106. https://www.sciencedirect.com/science/article/pii/S0277379115000360

77. **Revil**, A., Grauls, D., and Brévart, O. (**2002**). Mechanical compaction of sand/clay mixtures, J. Geophys. Res.-Sol. Ea., 107, 2293, https://doi.org/10.1029/2001JB000318

78. **Roelvink**, D., Reniers, A., Van Dongeren, A. P., De Vries, J. V. T., McCall, R., & Lescinski, J. (**2009**). Modelling storm impacts on beaches, dunes and barrier islands. *Coastal engineering*, *56*(11-12), 1133-1152. https://doi.org/10.1016/j.coastaleng.2009.08.006

79. **Rovere**, A., Raymo, M. E., Vacchi, M., Lorscheid, T., Stocchi, P., Gomez-Pujol, L., ... & Hearty, P. J. (**2016**). The analysis of Last Interglacial (MIS 5e) relative sea-level indicators: Reconstructing sea-level in a warmer world. Earth-Science Reviews, 159, 404-427. https://doi.org/10.1016/j.earscirev.2016.06.006

80. **Rovere**, A., Ryan, D. D., Vacchi, M., Dutton, A., Simms, A. R., & Murray-Wallace, C. V. (**2023**). The World Atlas of Last Interglacial Shorelines (version 1.0). Earth System Science Data, 15(1), 1-23. https://doi.org/10.5194/essd-15-1-2023, 2023

81. **Seard**, C., Borgomano, J., Granjeon, D., & Camoin, G. (**2013**). Impact of environmental parameters on coral reef development and drowning: Forward modelling of the last deglacial reefs from Tahiti (French Polynesia; IODP Expedition# 310). *Sedimentology*, *60*(6), 1357-1388. https://doi.org/10.1111/sed.12030

82. **Speed**, R. C., & **Cheng**, H. (**2021**). *Emergence and Evolution of Barbados* (Vol. 549). Geological Society of America.

83. **Toomey**, M., Ashton, A.D. & Perron, J.T. (**2013**) Profiles of ocean island coral reefs controlled by sea-level history and carbonate accumulation rates. Geology, 41(7), 731–734. https://doi.org/ 10.1130/G34109.1

84. **Trenkamp**, R., Kellogg, J. N., Freymueller, J. T., & Mora, H. P. (**2002**). Wide plate margin deformation, southern Central America and northwestern South America, CASA GPS observations. *Journal of South American Earth Sciences*, *15*(2), 157-171. https://doi.org/10.1016/S0895-9811(02)00018-4

85. **Turcotte**, D.L. & **Bernthal**, M.J. (**1984**) Synthetic coral-reef terraces and variations of Quaternary sea level. Earth and Planetary Science Letters, 70(1), 121–128. https://doi.org/10.1016/0012-821X(84)90215-2

86. **Van Duyl**, F. C. (**1985**). Atlas of the Living Reefs of Cura «; ao and Bonaire (Netherlands Antilles). *Foundation for Scientific Research in Surinam and the Netherlands Antilles*, *117*.

87. **Waelbroeck**, C., Labeyrie, L., Michel, E., Duplessy, J. C., Mcmanus, J. F., Lambeck, K., ... & Labracherie, M. (**2002**). Sea-level and deep water temperature changes derived from benthic foraminifera isotopic records. Quaternary science reviews, 21(1-3), 295-305. https://doi.org/10.1016/S0277-3791(01)00101-9

88. **Warrlich**, G. M. D., Waltham, D. A., & Bosence, D. W. J. (**2002**). Quantifying the sequence stratigraphy and drowning mechanisms of atolls using a new 3-D forward stratigraphic modelling program (CARBONATE 3D). *Basin Research*, *14*(3), 379-400. https://doi.org/10.1046/j.1365-2117.2002.00181.x

89. **Webster**, J.M., Wallace, L.M., Clague, D.A. & Braga, J.C. (**2007**) Numerical modeling of the growth and drowning of Hawaiian coral reefs during the last two glacial cycles (0-250 kyr). Geochemistry, Geophysics, Geosystems, 8(3), n/a. https://doi.org/10.1029/2006GC001415

90. **White**, R. V., Tarney, J., Kerr, A. C., Saunders, A. D., Kempton, P. D., Pringle, M. S., & Klaver, G. T. (**1999**). Modification of an oceanic plateau, Aruba, Dutch Caribbean: implications for the generation of continental crust. *Lithos*, *46*(1), 43-68. https://doi.org/10.1016/S0024-4937(98)00061-9

91. **Williams**, H.D., Burgess, P., Wright, V.P., Della Porta, G. and Granjeon, D. (**2011**) Understanding carbonate platform types: multiple controls and a continuum of geometries. J. Sed. Res., 81, 18–37.

Journal of Geophysical Research: Earth Surface

Supporting Information for

Unravelling the spatial variability of fossil coral reef morphology on Aruba and the implications for paleo sea level estimates

Denovan Chauveau*[a,b], Patrick Boyden[c], Florent Desfromont[d], Giovanni Scardino[e,f], Giovanni Scicchitano[e,f], Eric Mijts[g], Sonia Bejarano[h], Silas Dean[b], Ciro Cerrone[b], Alessio Rovere[b,c]

[a] Geo-Ocean, Univ Brest, CNRS, Ifremer, UMR6538, F-29280 Plouzané, France
[b]Department of Environmental Sciences, Informatics and Statistics, Ca' Foscari University of Venice, Italy
[c]MARUM, Center for Marine Environmental Sciences, University of Bremen, Germany
[d]Beicip-Franlab, Rueil-Malmaison, France
[e]Department of Earth and Geo-environmental Sciences, University of Bari Aldo Moro, 70125 Bari, Italy
[f]Interdepartmental Research Center for Coastal Dynamics, University of Bari Aldo Moro, 70125 Bari, Italy
[g]University of Aruba, Oranjestad, Aruba
[h]Reef Systems Research Group, Leibniz Centre for Tropical Marine Research (ZMT), Bremen, Germany

Figures S1 to S5

Introduction

This supplementary information includes figures with the field observations (figures S1-S5).

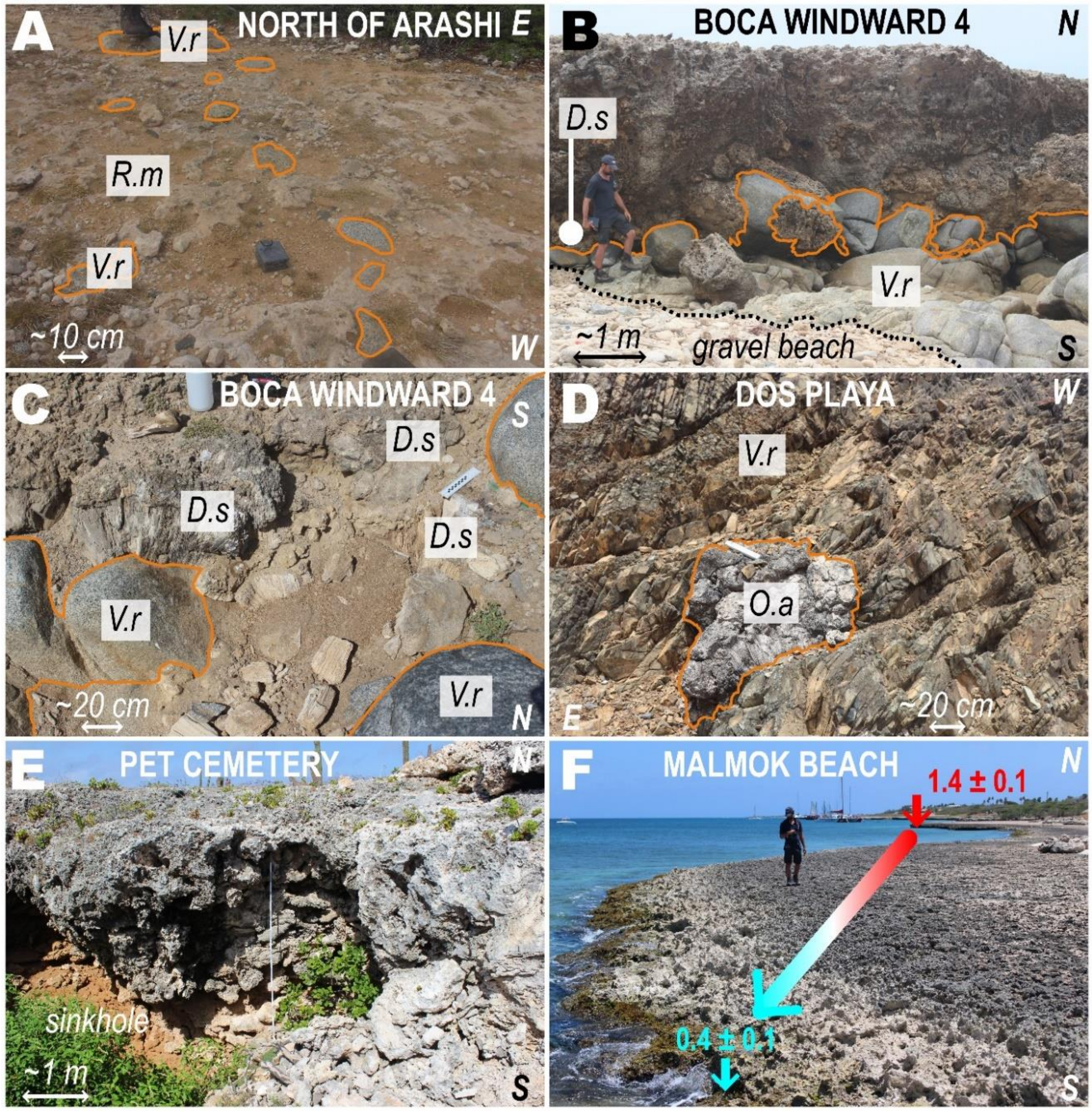

Figure S1. *Photo of contacts between CRT I and volcanic basement rocks, for* ***A)*** *leeward and* ***B-C)*** *windward at Boca Windward 4,* ***D)*** *Dos Playa.* ***E)*** *Pet cemetery and F) Malmok Beach sites. Contact zones are marked by the brown line. The designated corals are all in a living-growth position. The acronyms are defined as follows: D.s.:* Diploria strigosa; *O.a.;* Orbicella annularis; *V.r.: Volcanic rock; R.m.: Reef matrix. The elevations are from the dGNSS transects.*

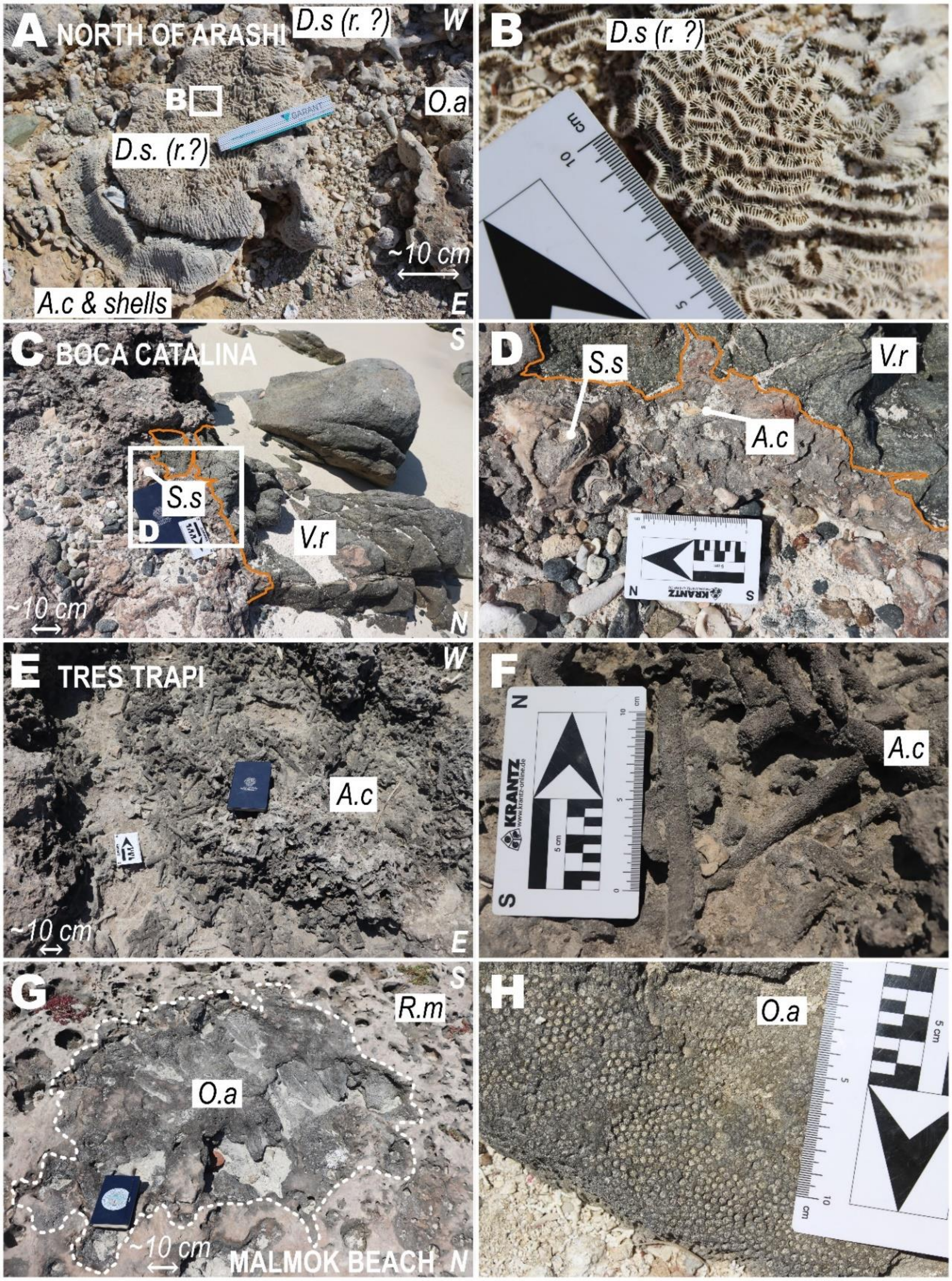

Figure S2. *CRT 1 details in leeward side of Aruba, from the north to the south, at* ***A-B)*** *Arashi Dune,* ***C-D)*** *Boca Catalina,* ***E-F)*** *Tres Trapi, and* ***G-H)*** *Malmok Beach. See location on Figure 2. The acronyms are defined as follows: D.s.:* Diploria strigosa*; O.a.;* Orbicella annularis*; A.c.:* Acropora cervicornis*; S.s.:* Strombus strombus*; V.r.: Volcanic rock; R.m.: Reef matrix. The pictures on the right (B, D, F, and H) are close-ups of the photos on the left (A, C, E, and G). The brown line marks the contact between the reef limestones and the volcanic basement.*

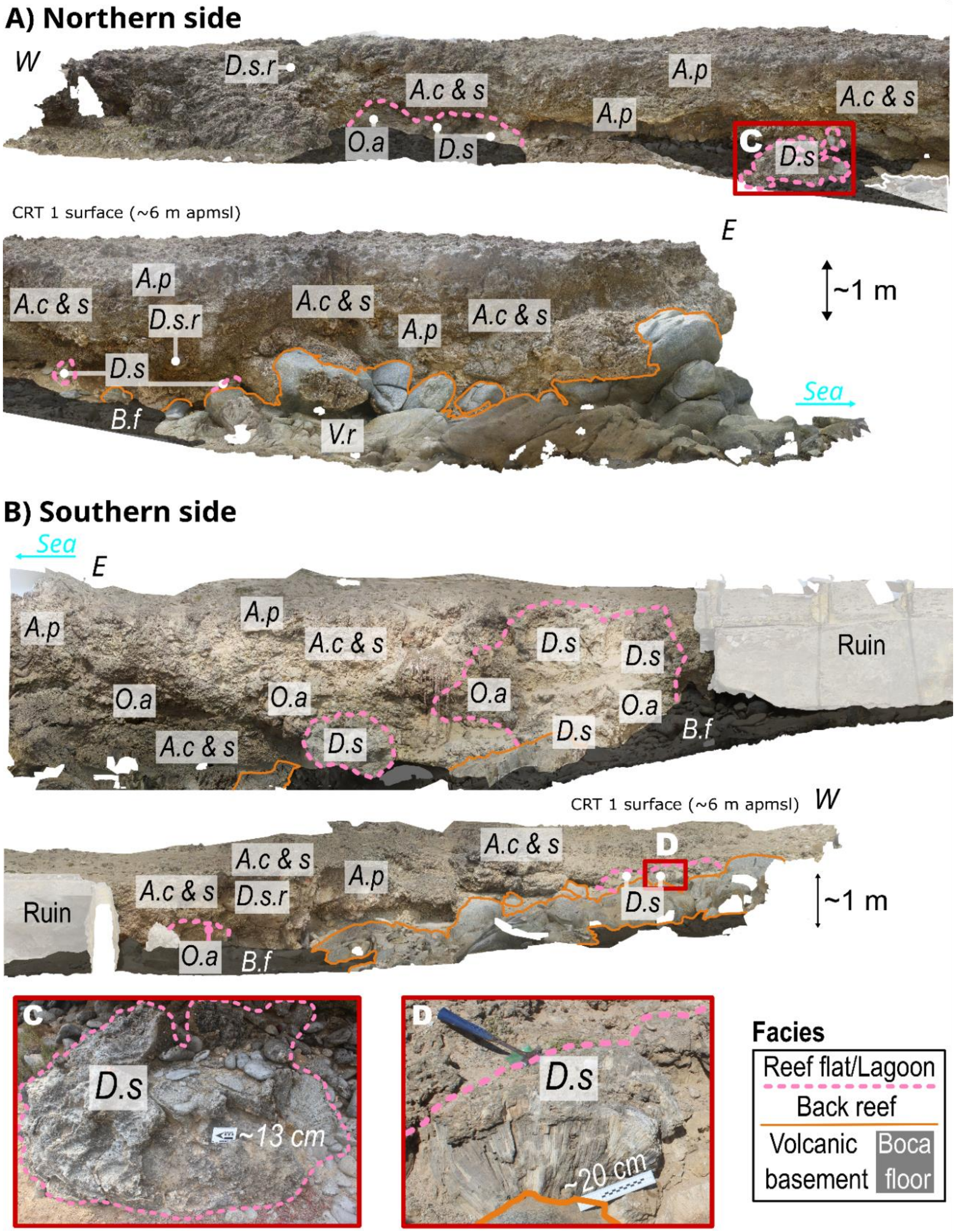

Figure S3. *Photogrammetric surveys of the CRT I in Boca Windward 4 (windward side of Aruba).* ***A)*** *Northern and* ***B)*** *Southern sides of the Boca. See location on Figure 2. The acronyms are defined as follows: D.s.:* Diploria strigosa*; O.a.;* Orbicella annularis*; A.c.:* Acropora cervicornis*; A.p.:* Acropora palmata*; V.r.: Volcanic rock; B.f.: Boca floor; s.: shell; r.: reworked.*

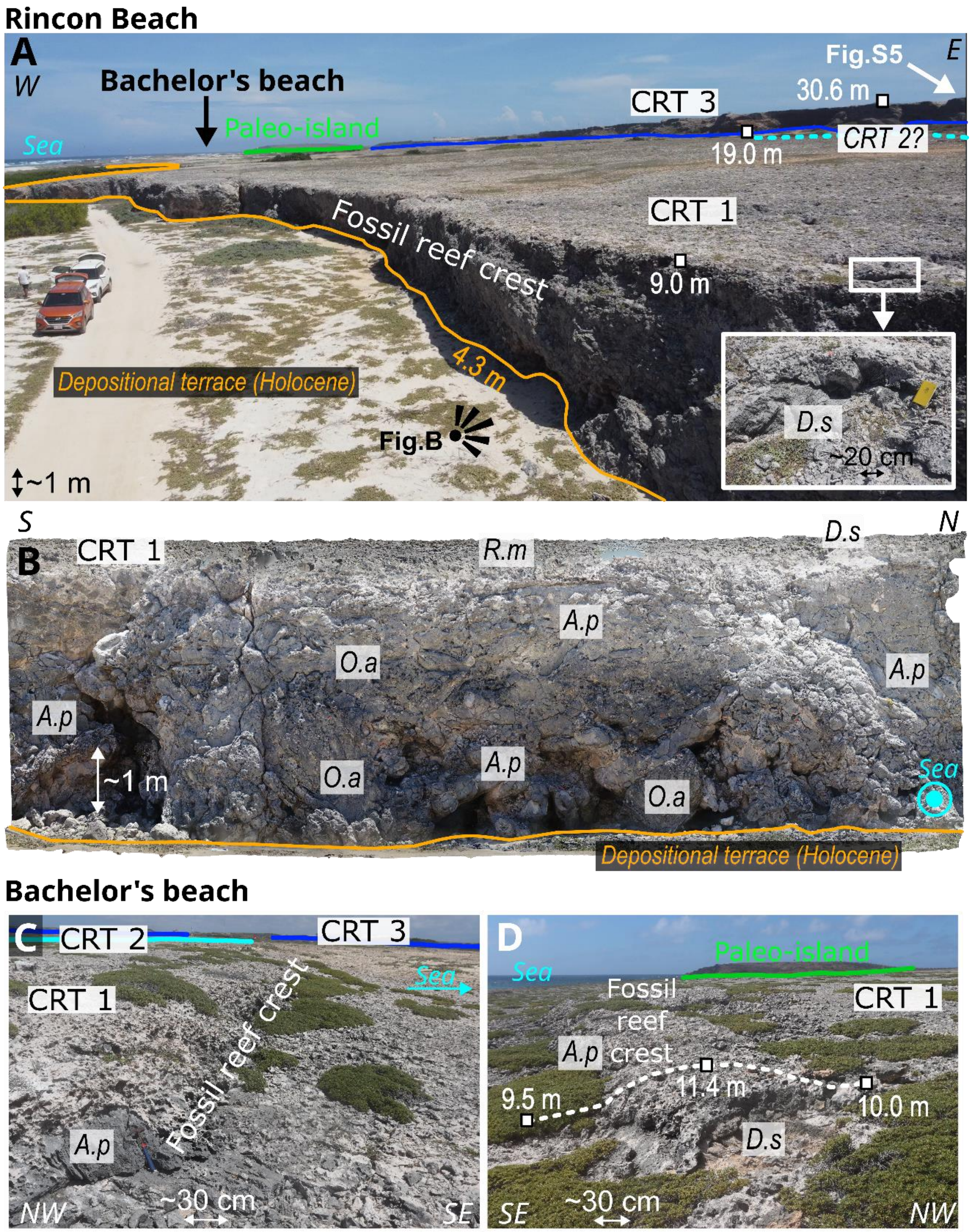

Figure S4. *Observed coral reef facies in* ***A-B)*** *Rincon beach Aruba and* ***C-D)*** *Bachelor's beach. A) is a drone view and B) a photogrammetric survey. See location on Figure 2. The acronyms are defined as follows: D.s.:* Diploria strigosa*; O.a.:* Orbicella annularis*; A.p.:* Acropora palmata*. All the corals were observed in a living-growth position. The elevations are from the dGNSS transects, have an uncertainties of ±0.1 m and are relative to the msl.*

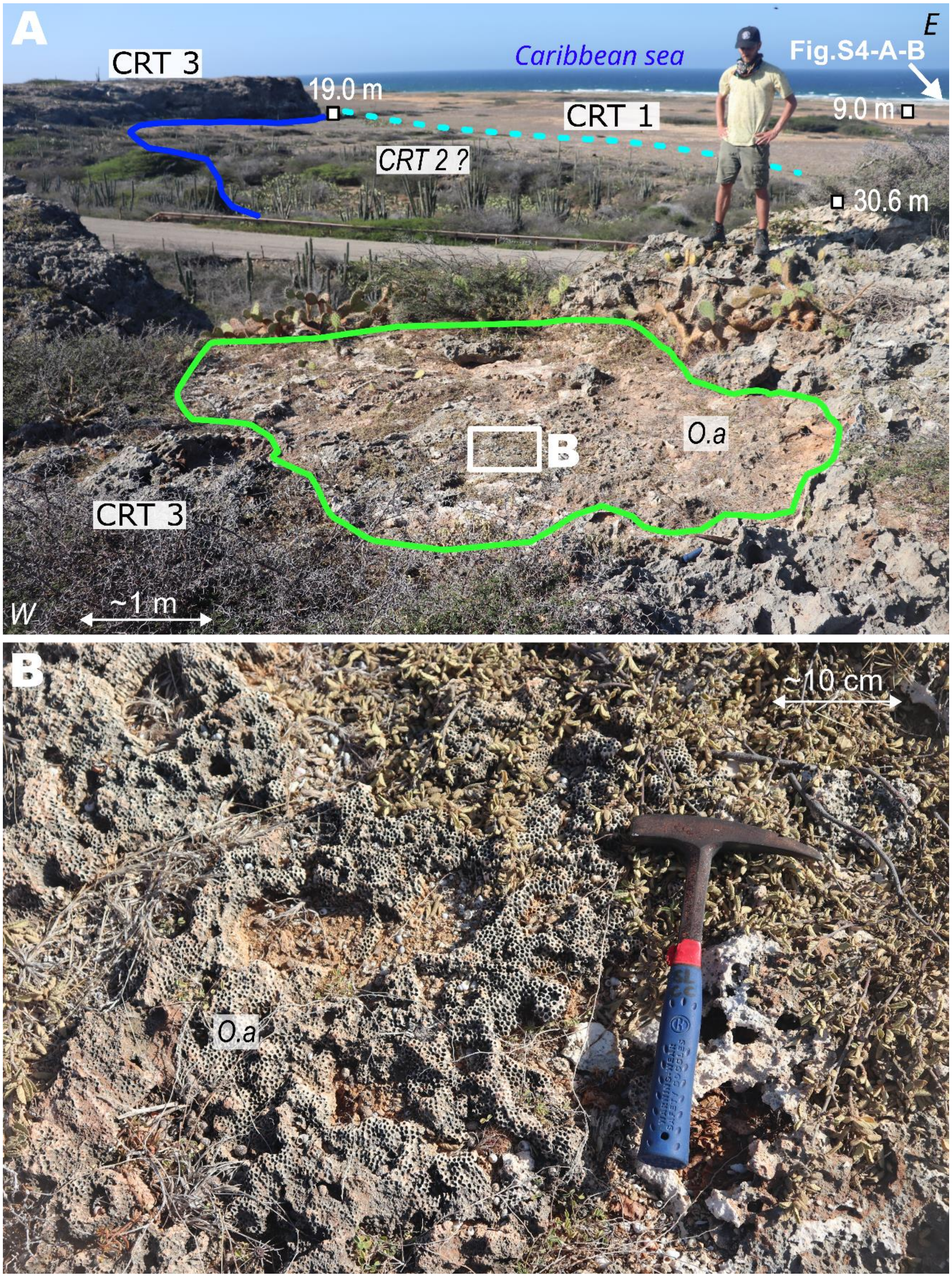

Figure S5. *Observed coral reef terrace in Rincon beach.* ***A)*** *Distal edge of CRT 3 (MIS 11?) with a coral colony (*O.a.: O. Annularis*) several meters wide (delimited by the green line).* ***B)*** *Close-up of the coral colony. The elevations are from the dGNSS transects, have an uncertainties of ±0.1 m and are relative to the msl.*

Journal of Geophysical Research: Earth Surface

Supporting Information for

Unravelling the spatial variability of fossil coral reef morphology on Aruba and the implications for paleo sea level estimates

Denovan Chauveau*[a,b], Patrick Boyden[c], Florent Desfromont[d], Giovanni Scardino[e,f], Giovanni Scicchitano[e,f], Eric Mijts[g], Sonia Bejarano[h], Silas Dean[b], Ciro Cerrone[b], Alessio Rovere[b,c]

[a] Geo-Ocean, Univ Brest, CNRS, Ifremer, UMR6538, F-29280 Plouzané, France
[b]Department of Environmental Sciences, Informatics and Statistics, Ca' Foscari University of Venice, Italy
[c]MARUM, Center for Marine Environmental Sciences, University of Bremen, Germany
[d]Beicip-Franlab, Rueil-Malmaison, France
[e]Department of Earth and Geo-environmental Sciences, University of Bari Aldo Moro, 70125 Bari, Italy
[f]Interdepartmental Research Center for Coastal Dynamics, University of Bari Aldo Moro, 70125 Bari, Italy
[g]University of Aruba, Oranjestad, Aruba
[h]Reef Systems Research Group, Leibniz Centre for Tropical Marine Research (ZMT), Bremen, Germany

Figures S6 to S29

Introduction

Below are the 3D blocks modelled for each scenario in the three domains (leeward, windward and south). The facies defined in Section 3.2.7 are shown. The wells shown in Figure 7 of the main manuscript are located in each figure. The figures represent the raw output of the DionisosFlow software. The X and Y grids correspond to UTM coordinates. The Z axis is the relative elevation with respect to the first iteration of sea level value at 400 ka. It is therefore necessary to add 3.2 m and 23.2 m to the Z values for the scenarios without and with uplift, respectively.

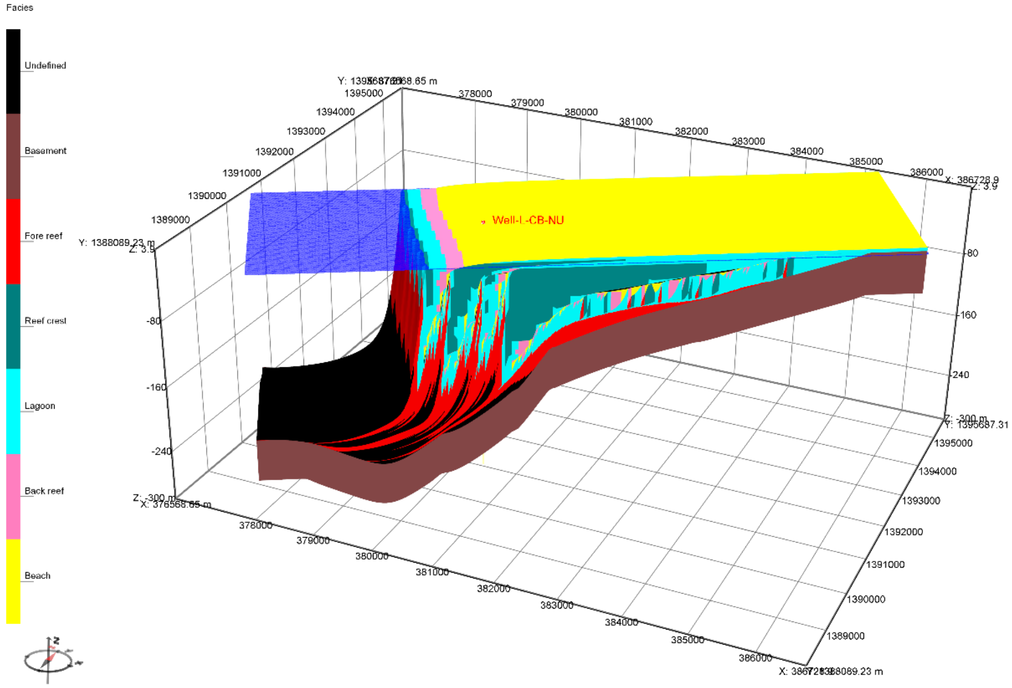

Figure S6. *Model output (facies) from the CB-NU scenario for the leeward domain.*

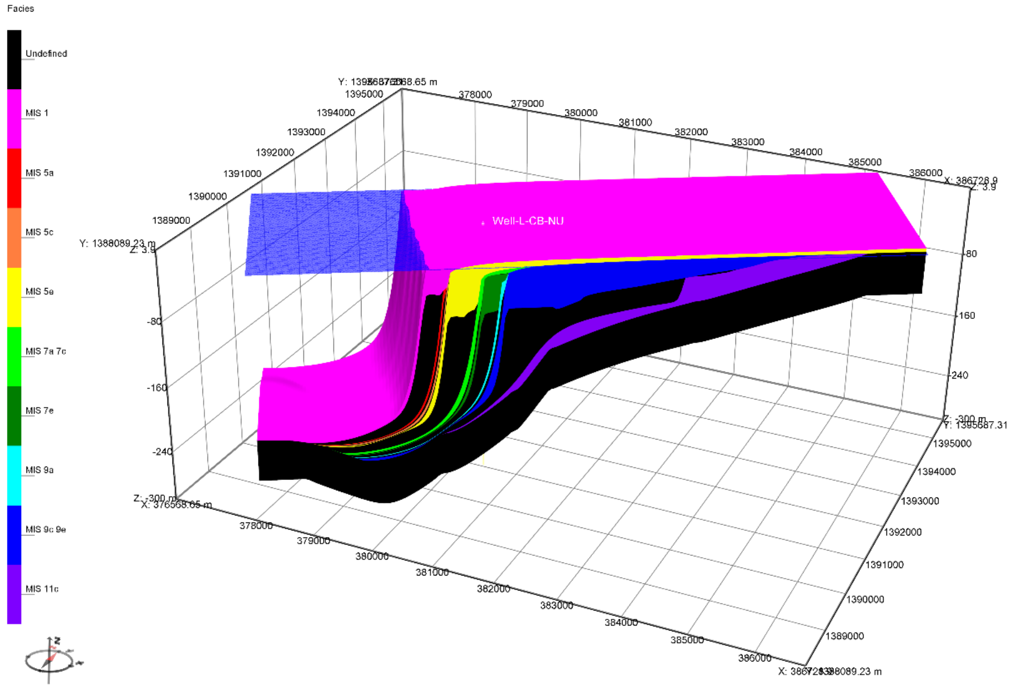

Figure S7. *Model output (MIS) from the CB-U scenario for the leeward domain.*

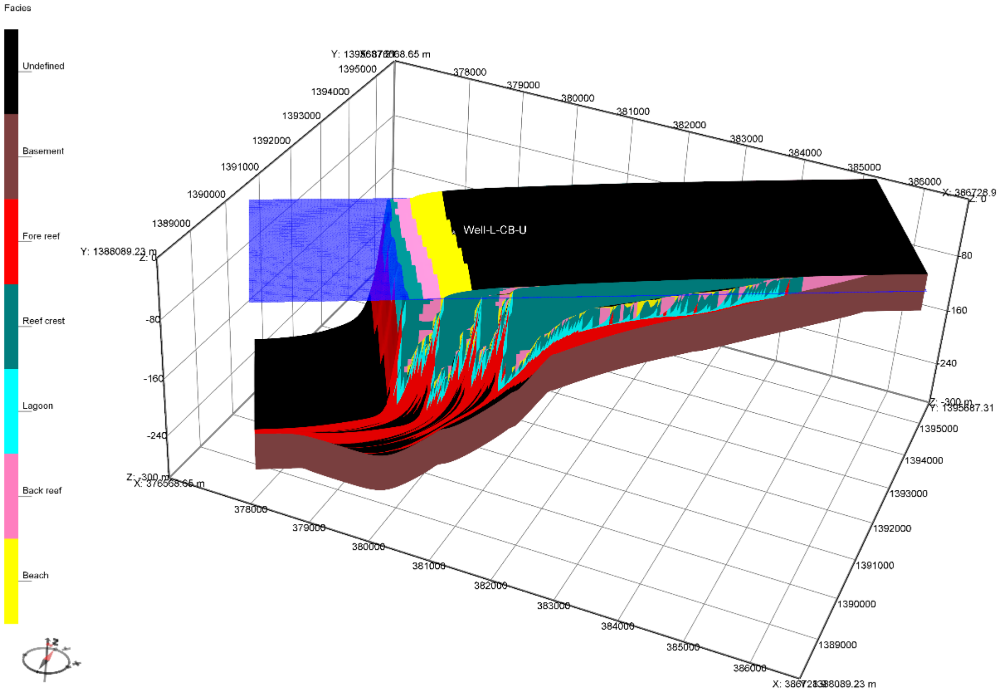

Figure S8. Model output (facies) from the CB-U scenario for the leeward domain.

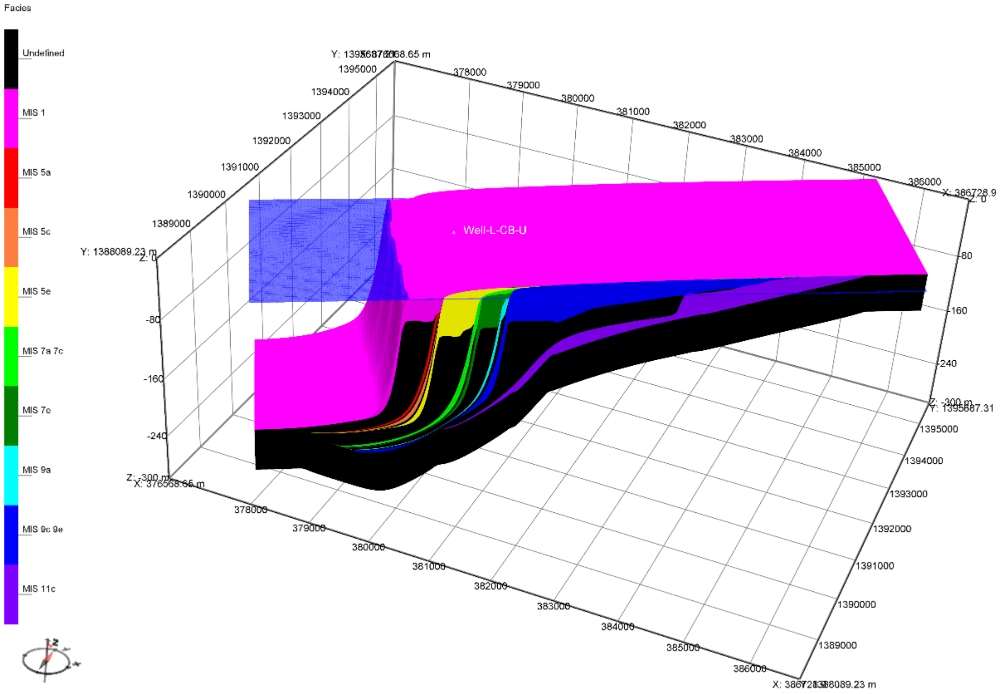

Figure S9. Model output (MIS) from the CB-U scenario for the leeward domain.

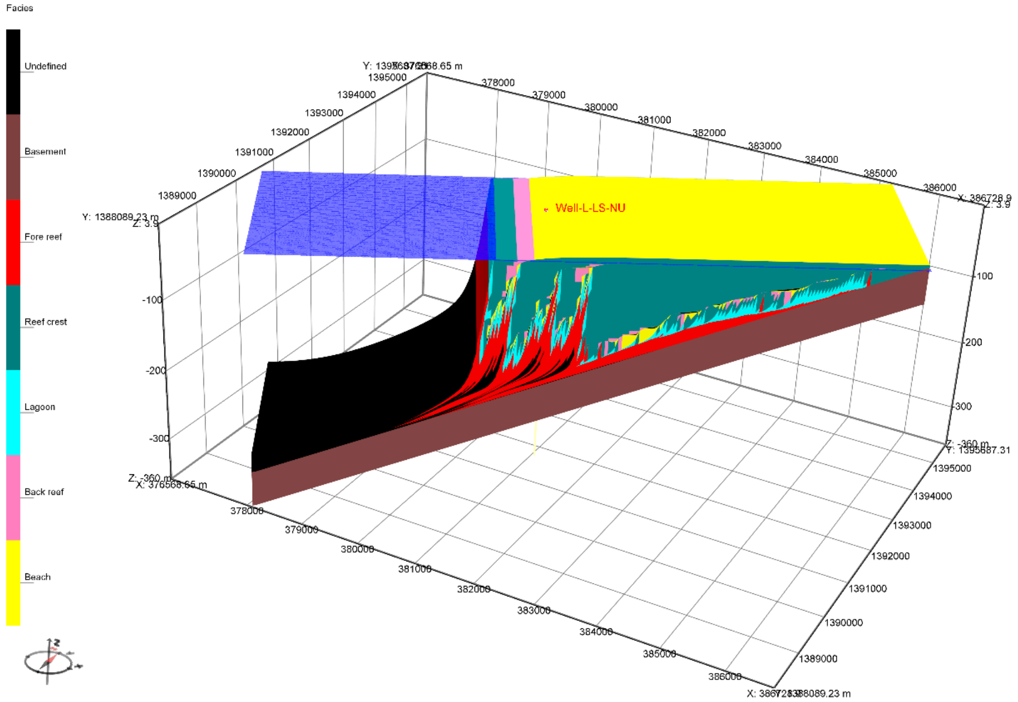

Figure S10. *Model output (facies) from the LS-NU scenario for the leeward domain.*

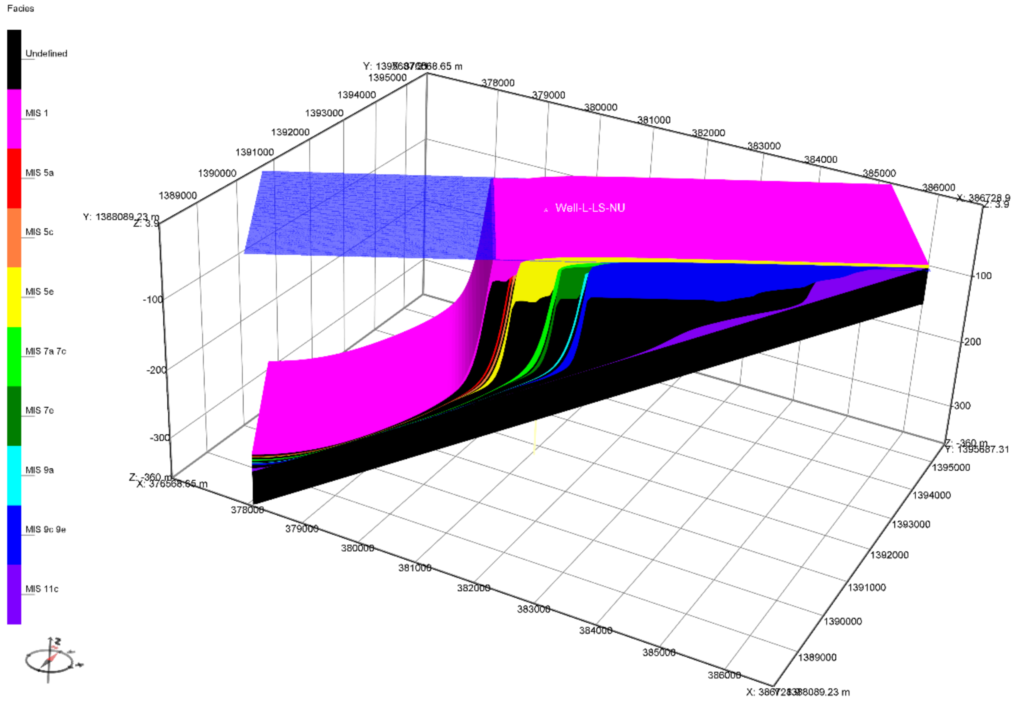

Figure S11. *Model output (MIS) from the LS-NU scenario for the leeward domain.*

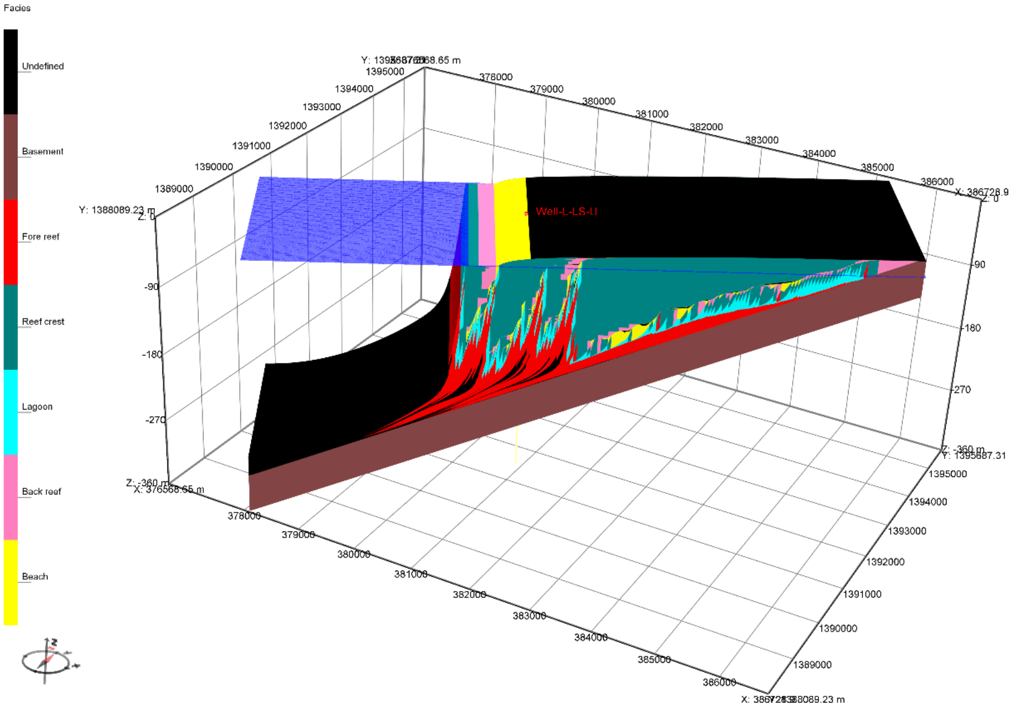

Figure S12. *Model output (facies) from the LS-U scenario for the leeward domain.*

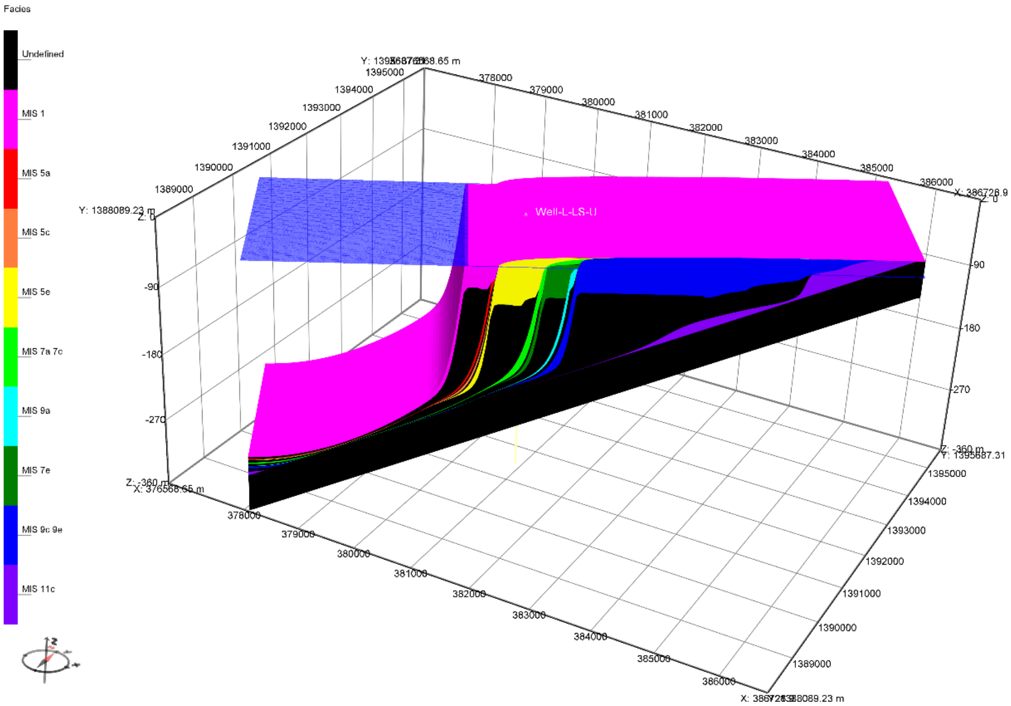

Figure S13. *Model output (MIS) from the LS-U scenario for the leeward domain.*

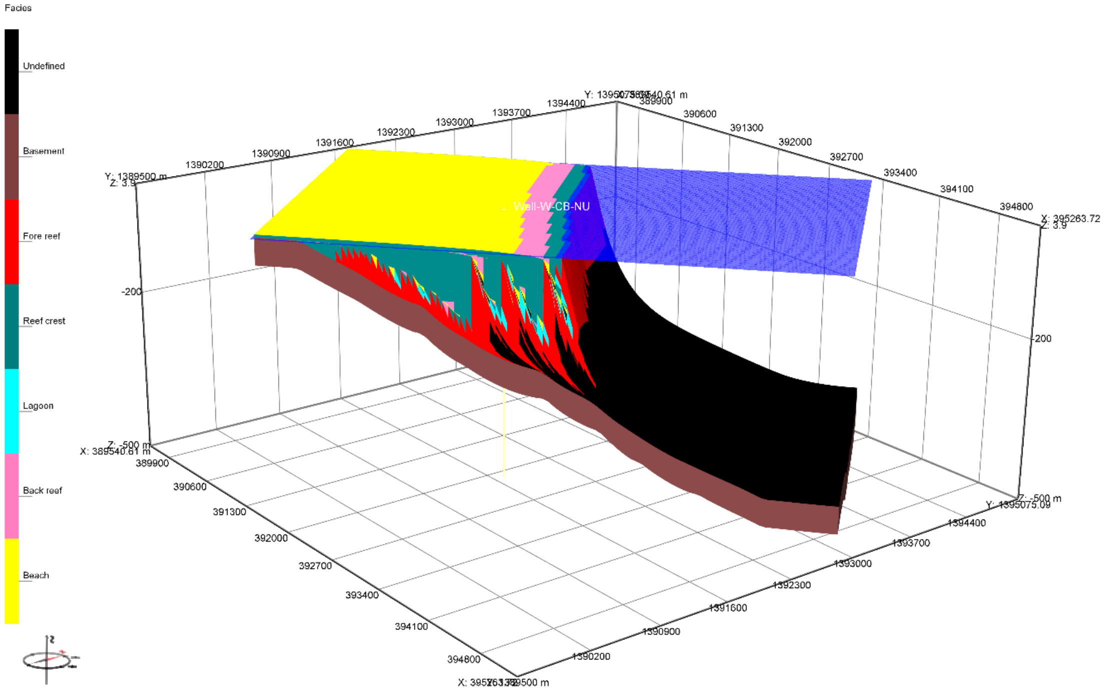

Figure S14. *Model output (facies) from the CB-NU scenario for the windward domain.*

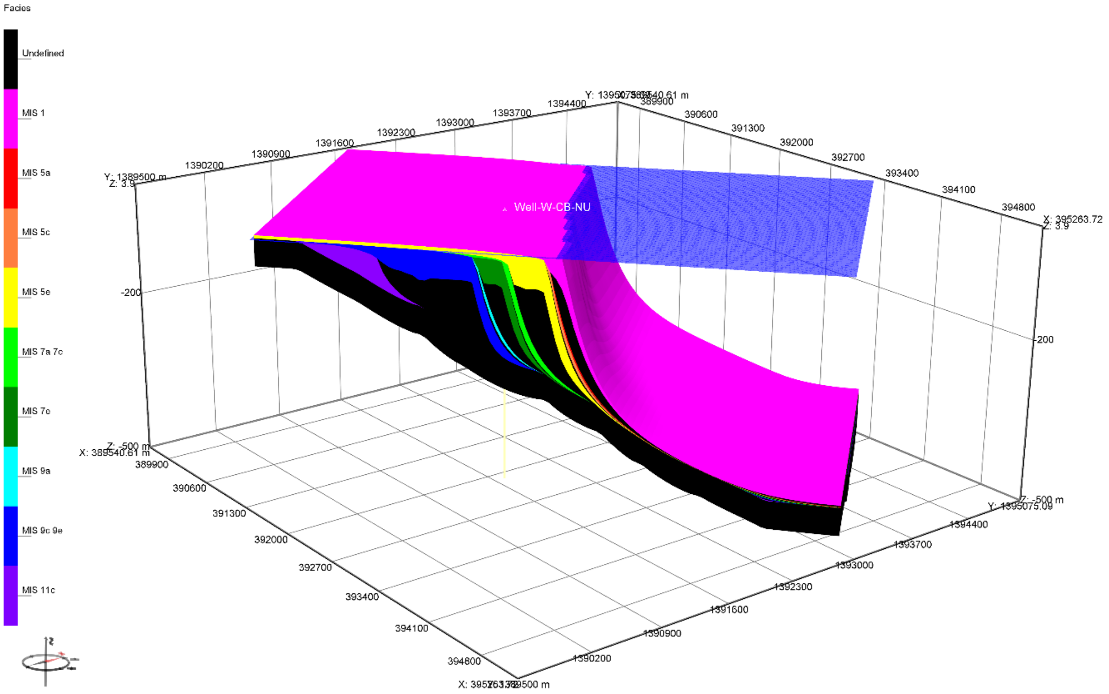

Figure S15. *Model output (MIS) from the CB-NU scenario for the windward domain.*

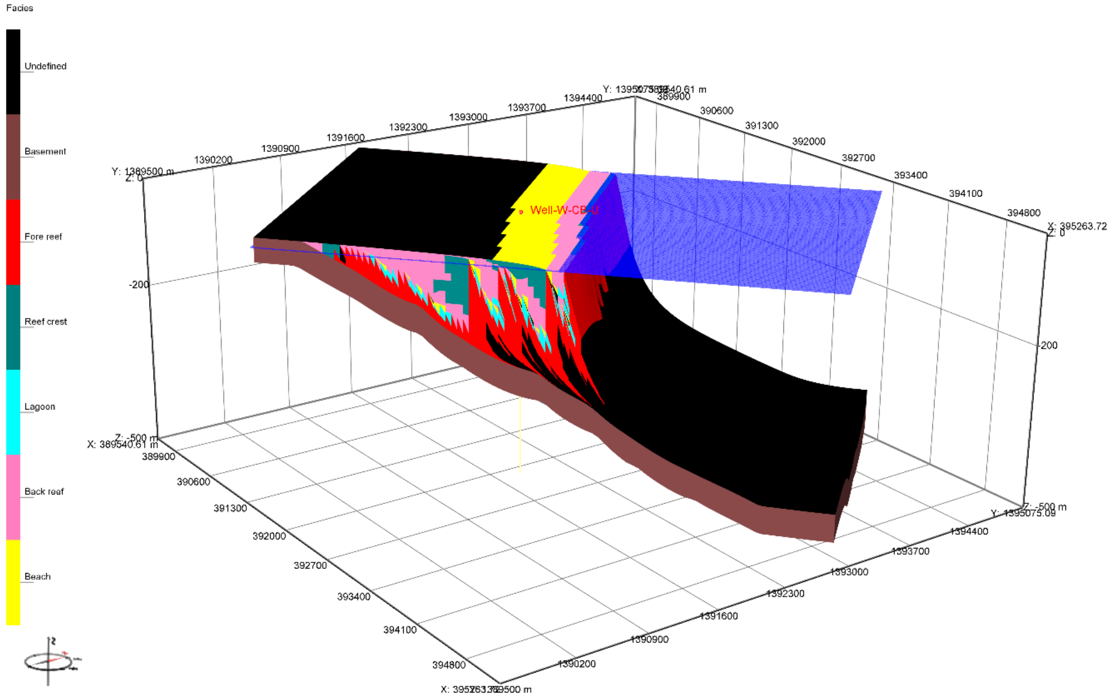

Figure S16. *Model output (facies) from the CB-U scenario for the windward domain.*

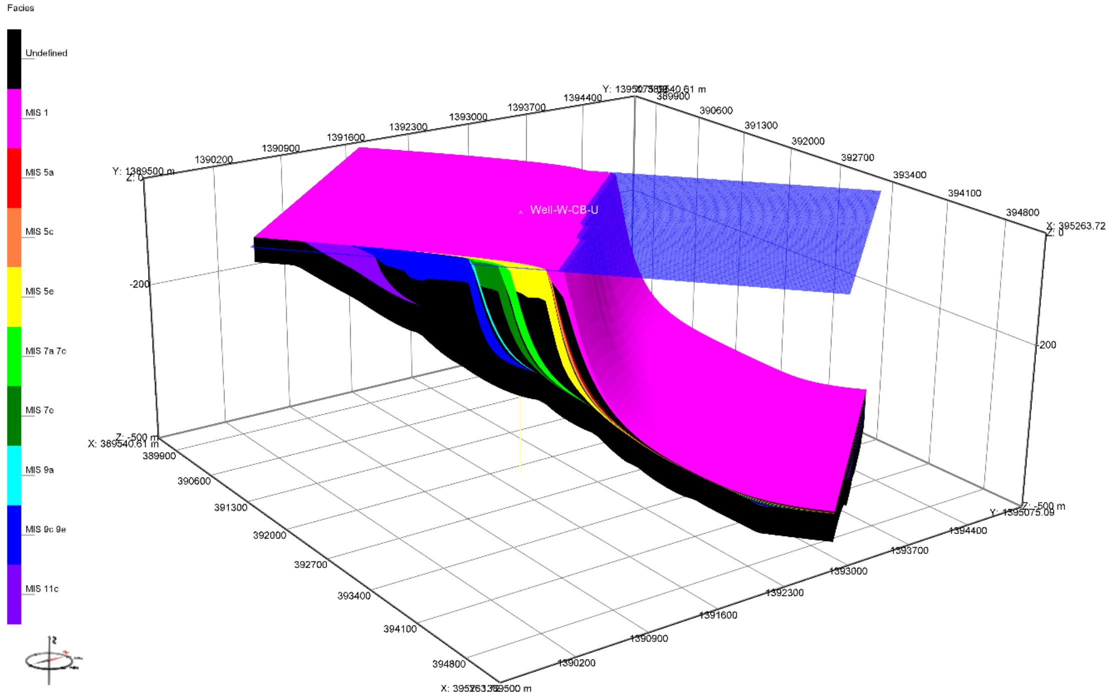

Figure S17. *Model output (MIS) from the CB-U scenario for the windward domain.*

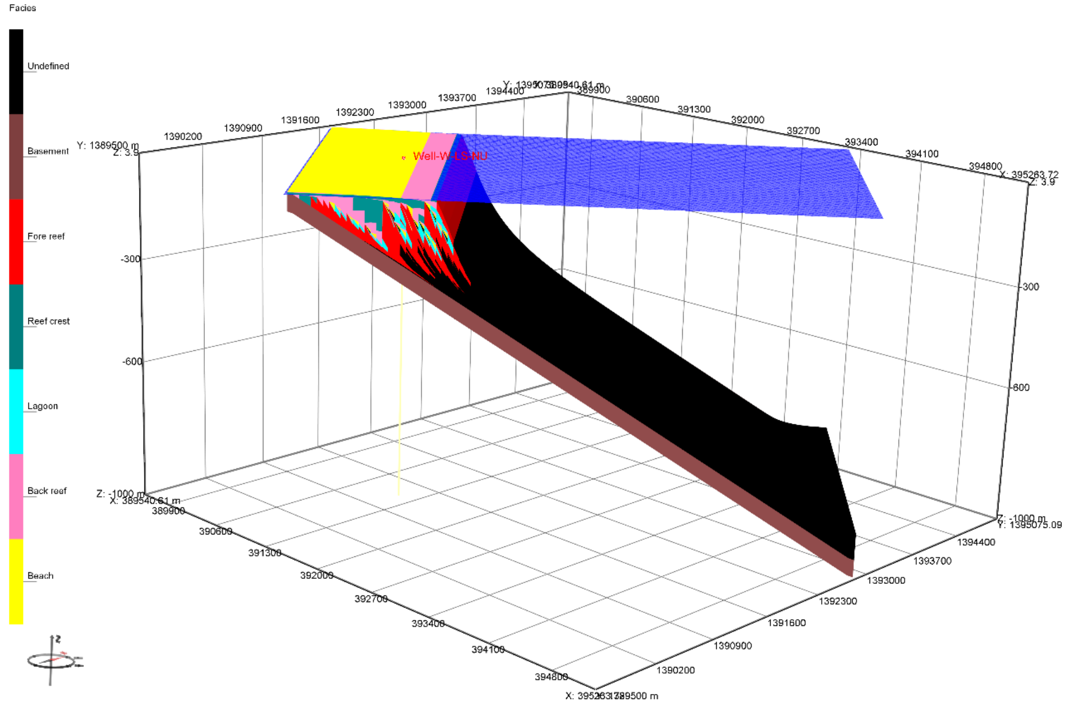

Figure S18. *Model output (facies) from the LS-NU scenario for the windward domain.*

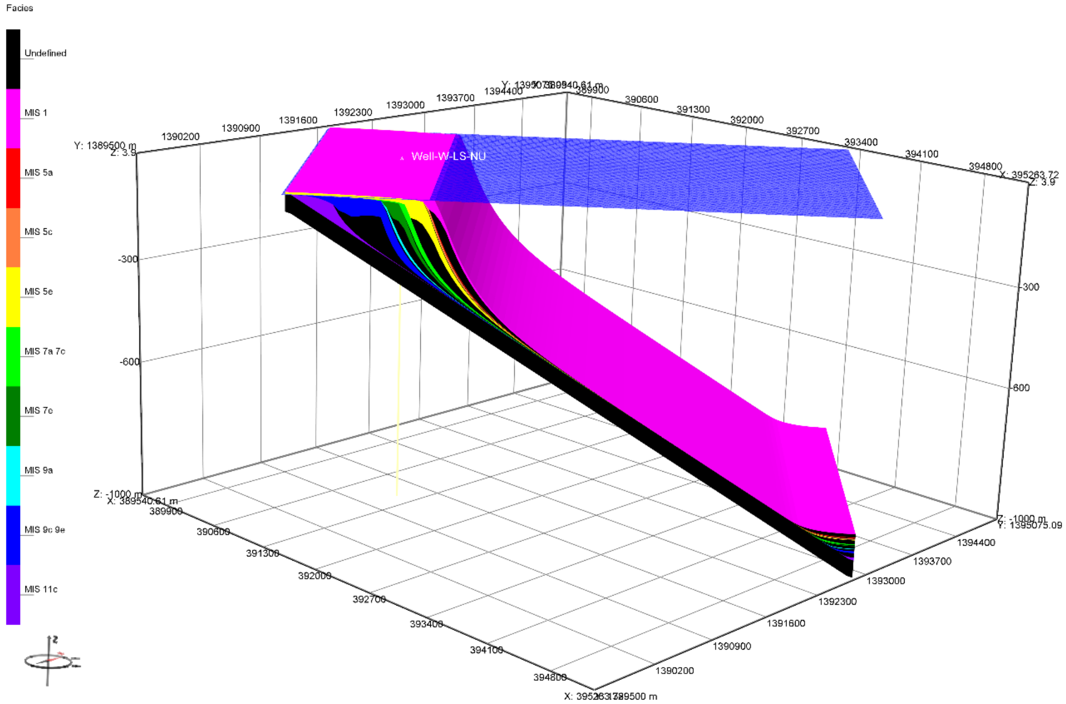

Figure S19. *Model output (MIS) from the LS-NU scenario for the windward domain.*

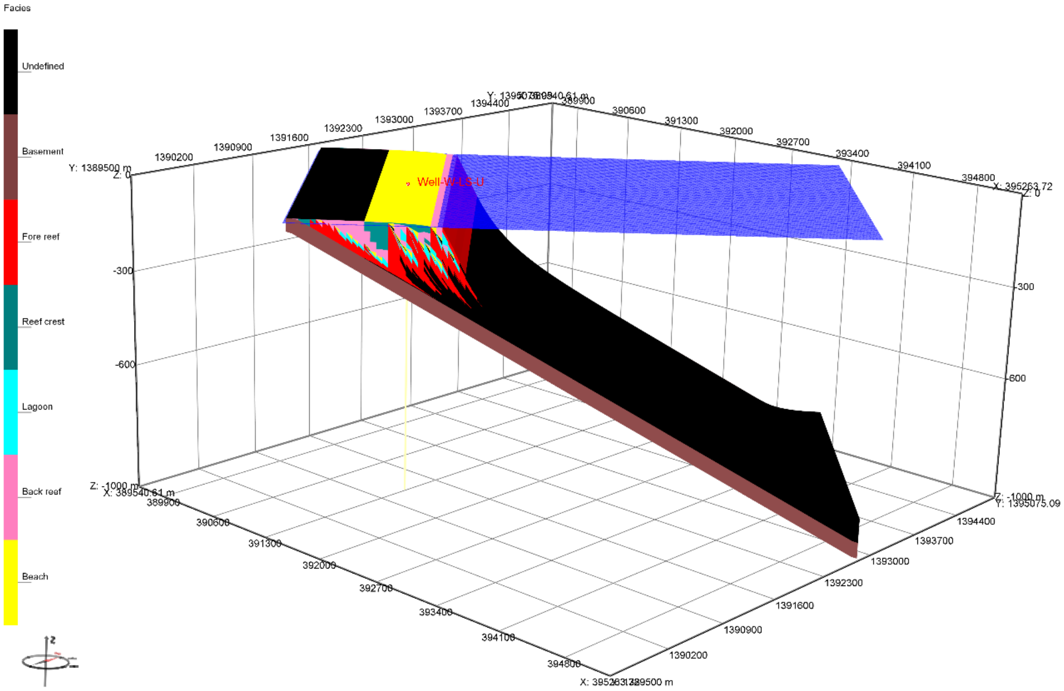

Figure S20. *Model output (facies) from the LS-U scenario for the windward domain.*

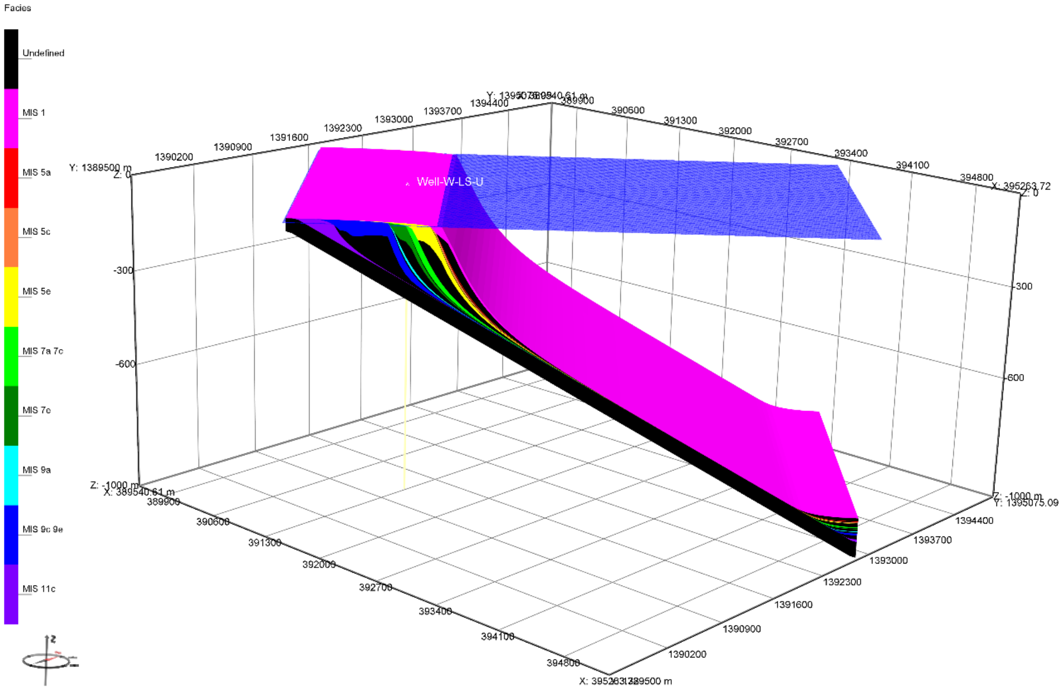

Figure S21. *Model output (MIS) from the LS-U scenario for the windward domain.*

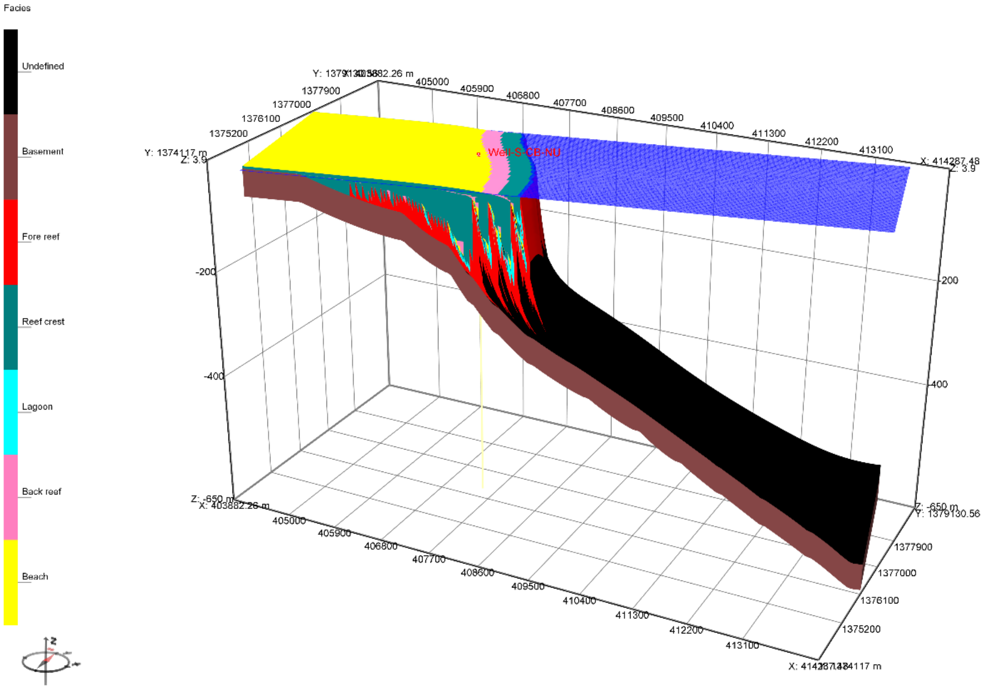

Figure S22. Model output (facies) from the CB-NU scenario for the southern domain.

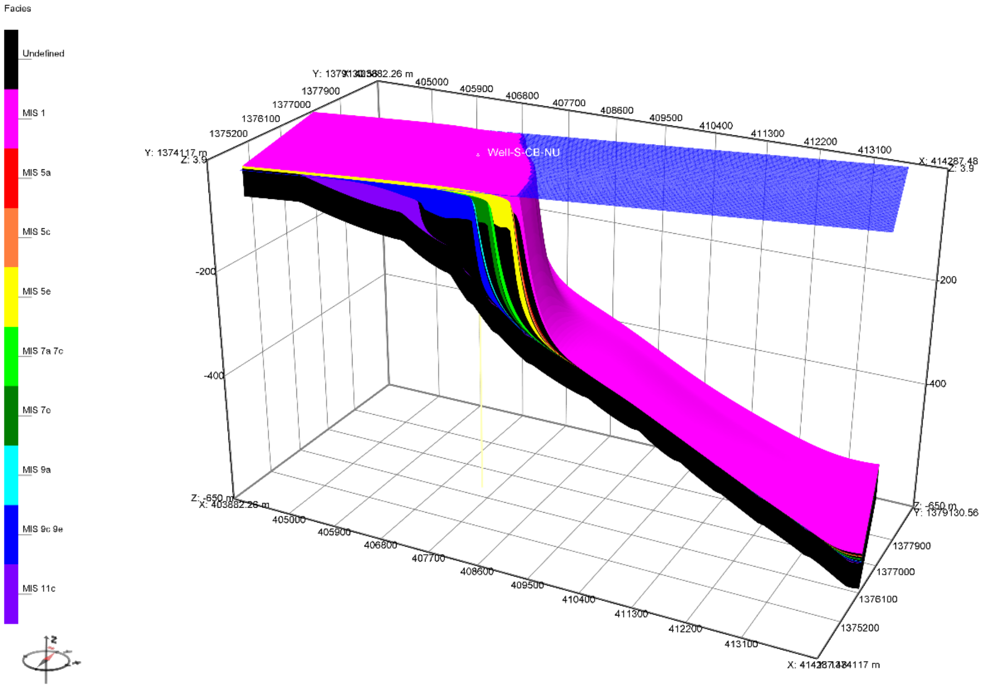

Figure S23. Model output (MIS) from the CB-NU scenario for the southern domain.

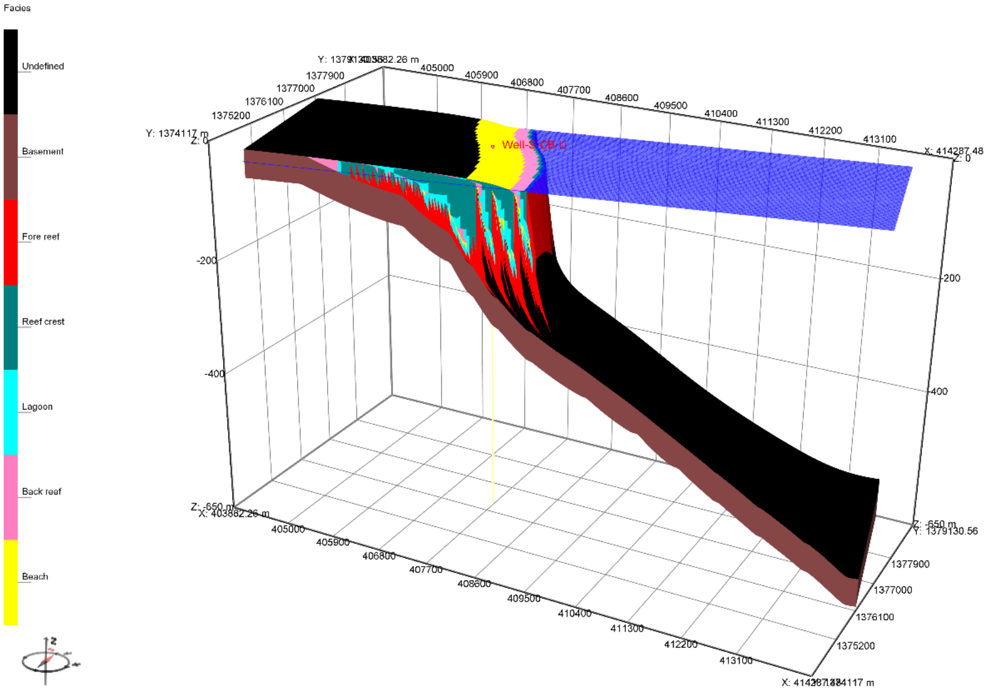

Figure S24. *Model output (facies) from the CB-U scenario for the southern domain.*

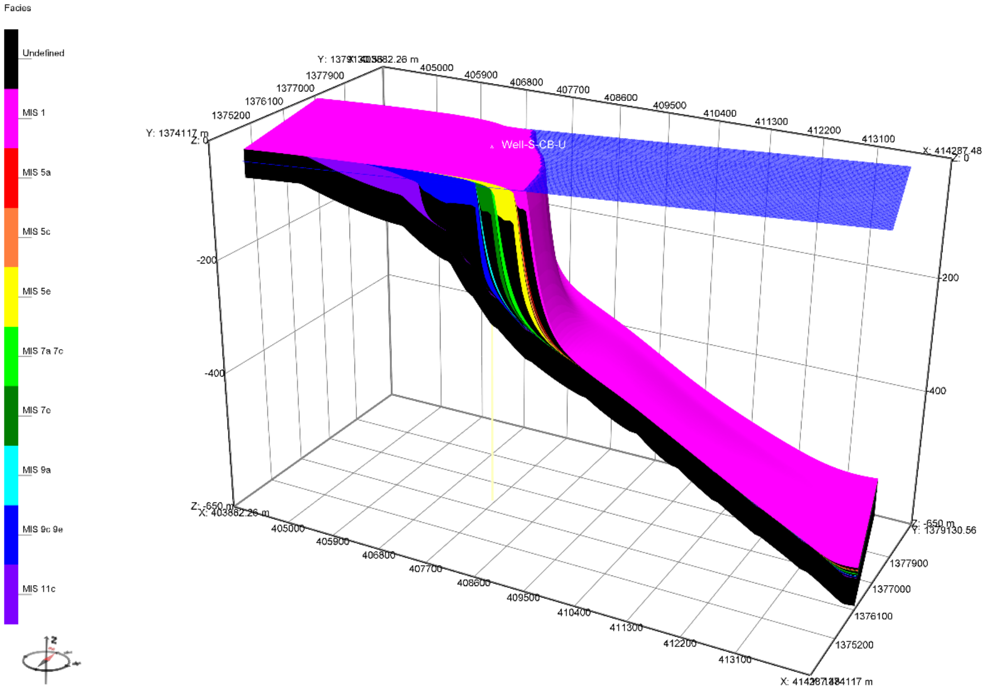

Figure S25. *Model output (MIS) from the CB-U scenario for the southern domain.*

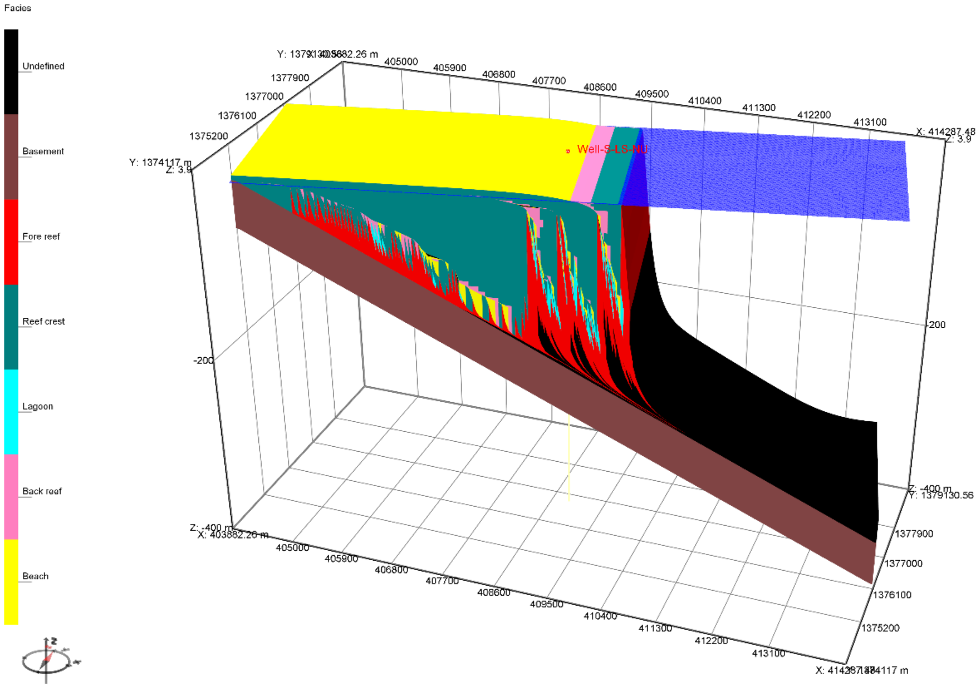

Figure S26. *Model output (facies) from the LS-NU scenario for the southern domain.*

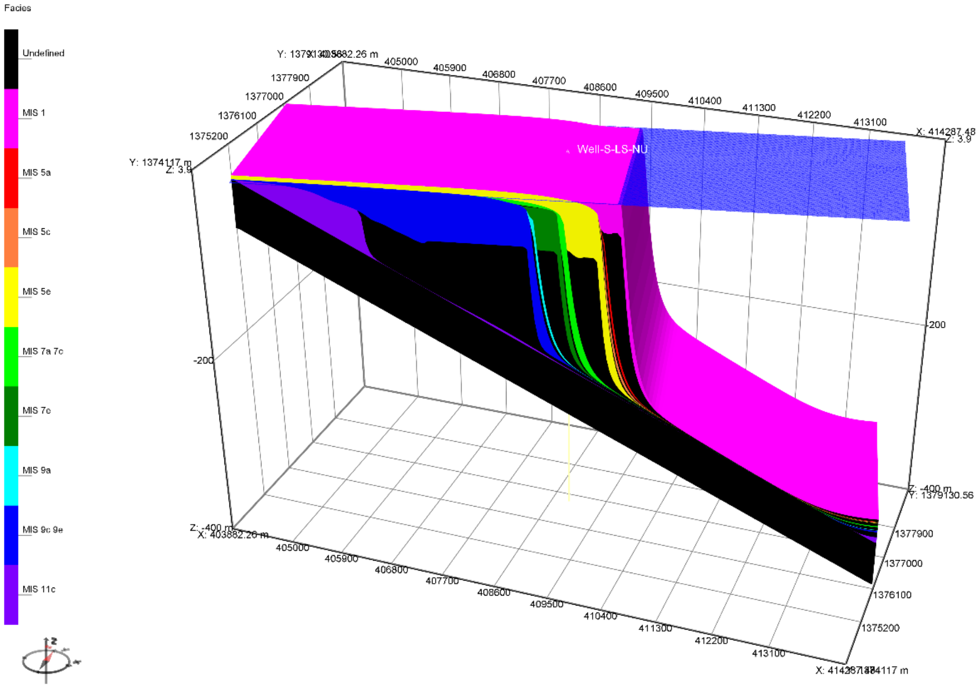

Figure S27. *Model output (MIS) from the LS-NU scenario for the southern domain.*

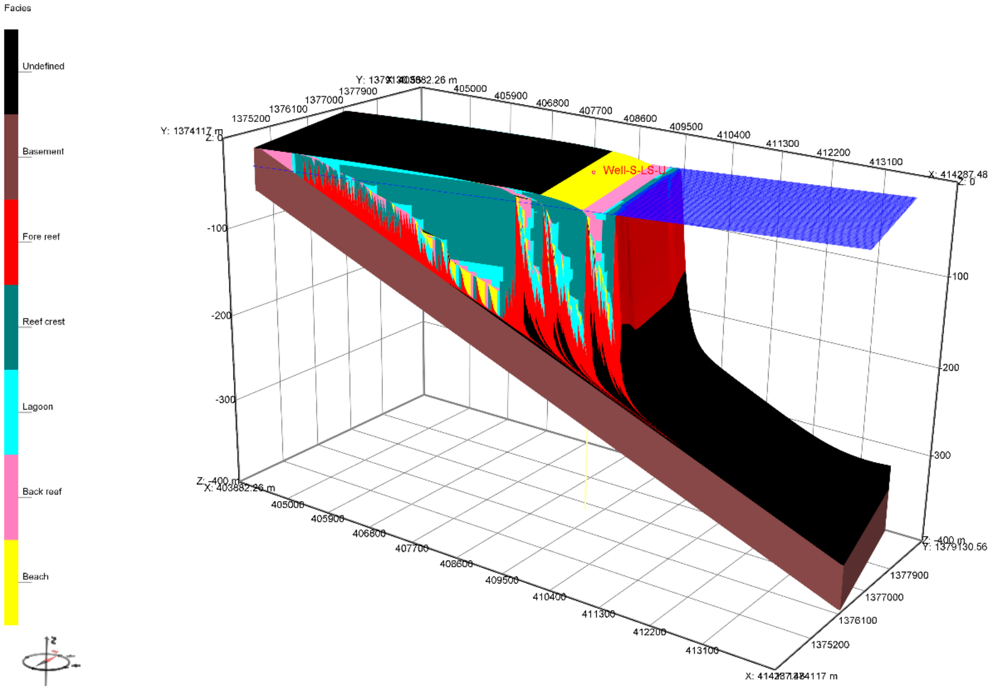

Figure S28. *Model output (facies) from the LS-U scenario for the southern domain.*

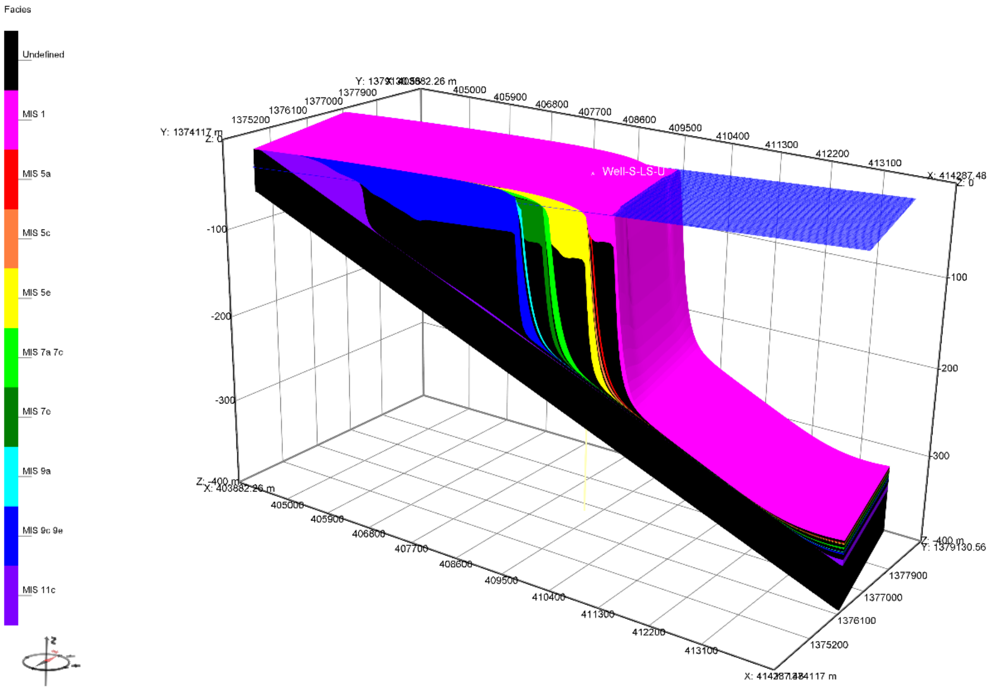

Figure S29. *Model output (MIS) from the LS-U scenario for the southern domain.*